A Chemoplastic Model for Alkali-Silica Expansion: Effect of Stress-Induced Anisotropy

ENG

by

Marcus G. Peterson

B.S. Civil Engineering
University of Minnesota

Submitted to the Department of Civil and Environmental Engineering
in partial fulfillment of the requirements for the Degree of
Master of Science
in Civil and Environmental Engineering

Massachusetts Institute of Technology

June 2000

Signature of Author_____
Department of Civil and Environmental Engineering
May 10, 2000

Certified by_____
Franz-Josef Ulm
Assistant Professor of Civil and Environmental Engineering
Thesis Supervisor

Accepted by_____
Professor Daniele Veneziano
Chairman, Departmental Committee on Graduate Studies

A Chemoplastic Model for Alkali-Silica Expansion: Effect of Stress-Induced Anisotropy

by
Marcus G. Peterson

Submitted to the Department of Civil and Environmental Engineering
on May 15, 2000 in partial fulfillment of the
requirements for the Degree of Master of Science in
Civil and Environmental Engineering

Abstract

The alkali-silica reaction (ASR) is an expansive chemical reaction that occurs between certain reactive aggregates and the alkaline pore solution surrounding them. In the presence of water, the volume of ASR products greatly exceeds that of the reactants, resulting in the generation of internal pressures that can cause substantial damage to civil engineering structures. This thesis aims to develop a model that employs principles of chemistry and mechanics to accurately predict the severity of ASR expansion with regard to material parameters and other relevant variables.

In this first chapter, the mechanisms of ASR expansion are first addressed and elucidated. Then, in Chapter 2, a literature review of past modeling attempts is presented. Finally, in Chapter 3, a new chemoplastic model of these mechanisms is formulated. Starting from energy considerations, this model includes a description of ASR kinetics, that is, an account of how the chemical reaction proceeds through time. Additionally, the model provides a link between reaction kinetics and material mechanics that finally can be extended to a structural level. This aspect of the modeling requires an understanding of the interaction between internal and external stresses that drive the expansive strain, by which the magnitude of ASR is measured. The chemoplastic model also incorporates another phenomenon observable in laboratory tests but not addressed in past literature, that of stress-induced anisotropy, which essentially states that the uniaxial restraint of ASR gel growth induces directionally preferential expansion of the gel. In other words, if the gel is restrained in one direction, it expands primarily in the stress-free directions.

Based on a chemomechanics approach, using the chemoplastic model and available experimental data, it is shown that the micromechanisms that lead to ASR swelling are the same as the ones activated during concrete fracture under macroscopic load application. This combined experimental-theoretical identification confirms both the model basis (chemoplasticity) and the capacity of the model to actually predict deleterious effects induced by the alkali-silica reaction in concrete structures. Finally, by way of conclusion, the model is calibrated with respect to test data obtained in the LCPC ASR test campaign by Larive, and the calibration is subsequently verified by a comparison of predicted and experimentally measured expansion curves.

Thesis Supervisor: Franz-Josef Ulm
Title: Assistant Professor, Department of Civil and Environmental Engineering

Acknowledgments

I would like to thank Professor Ulm, my thesis supervisor and advisor, for his guidance, encouragement, and enthusiasm. He always found the time to assist me with this research and answer my many questions, and his confidence in me was a great source of both motivation and inspiration.

I would also like to thank my family for providing me with support in this thesis and throughout my academic career.

Finally, I want to thank my fiancé, Amanda, for her infinite patience and support.

Contents

Chapter 1

ASR Mechanisms

In this chapter, the topic of ASR expansion is introduced first through a brief history of research on the phenomenon. Thereafter, based on a review of current literature, the chemistry of the reaction is examined. Finally, the mechanisms by which the reaction proceeds and causes structural damage are elucidated.

1.1 Historical Perspective

Of the three known types of deleterious alkali-aggregate reactions in concrete, the alkali-silica reaction is the most common. The other reactions, alkali-silicate and alkali-carbonate, can cause cracking and deterioration of concrete, but these reactions have not been as carefully studied and are not fully understood. Since alkali-silica reaction predominates alkali-aggregate reactions, this particular phenomenon has been examined more closely and is

better-understood [1]. T.E. Stanton first recognized and described the problem in a 1940 paper, following the observance of excessive expansion and cracking in a number of Californian structures in throughout the 1920's and 1930's. He attributed the deleterious reaction to the presence of specific mineral constituents within aggregates combined with a Portland cement rich in alkalis [2]. Stanton's discovery inspired much research over the next twenty years, but this work slowed substantially through the 1960's and the early 1970's. Due to increasing alkali contents in cement, new concrete manufacturing technologies, and the lack of superior quality aggregates, a resurgent interest in the problem has grown over the last twenty-five or so years [3]. During this time, a great deal of work has been done on the subject, and much has been learned.

1.2 Mechanisms of ASR

The ability of the ASR to proceed depends on the presence of three main variables:

1. Available alkalis from the cement clinker or other sources;
2. Reactive forms of silica within the aggregate;
3. Water.

Each of these criteria must be met for the reaction to occur [4]. The mechanism by which this reaction damages concrete is through the formation of a hydrophilic gel that swells and creates localized regions of great pressure that can initiate cracks [5]. Individual cracks tend to interconnect in larger networks in a pattern known as "map cracking" [6]. Since

the alkali-silica reaction can take ten years or better to develop [1], it may be many years before macrocracking in a concrete structure is observable. By this time little can be done to inhibit the onward progression of the reaction. Thus, it is advantageous to understand the mechanisms and chemistry of ASR, so deleterious occurrences of the reaction can be anticipated and prevented through judicious choices of materials.

1.3 Alkalis in Cement

The alkali-silica reaction actually takes place between reactive silica and hydroxides. However, the presence of alkali metals increases the hydroxide (OH^-) concentration, thus indirectly driving the so-called alkali-silica reaction [7]. Since the alkalis (namely K^+ and Na^+) are only partially incorporated into the hydration products of the cement, they are easily soluble in pore water [8]. Though the pH of the pore water during hydration is high (12 or greater), the alkalis dissolved from the cement clinker increase the hydroxide concentration even more (pH between 13 and 14) [7]. The presence of the alkalis can be traced in part to the calcination process in which the clinker is produced from raw materials. During this high-temperature procedure, K^+ and Na^+ (amongst some other materials) are vaporized due to their relatively high vapor pressures. While the clinker is slowly transported through the kiln, the vapor flows and eventually condenses onto the clinker, coating it with alkalis. Though the alkalis comprise a minor fraction of the resulting material, they ultimately play a most significant role in the alkali-silica reaction. While some of the alkalis remain on the surface of the clinker, others are locked within the structure of the clinker. Of those alkalis

within the hydrating concrete, the ones coating the clinker surface will become available most quickly. The alkalis locked inside the clinker structure will become available after some degree of hydration has occurred [9]. The majority of alkalis in the cement are in the form of sulfates [10].

1.4 Reactive Silica in Aggregates

Determination of which aggregates will be silica-reactive in the field can be a challenging undertaking. Testing of aggregates begins with a full petrographic examination to determine the presence of certain reactive constituents. Though a necessary first step, this phase of aggregate testing may not provide much information, as the process of constituent identification can be quite arduous [11]. Further testing may provide more helpful data, but in fact there exists no reliable way of determining an aggregate's reactivity in the field. Many factors come into play in the characterization of the degree of reactivity. Such morphological traits as crystallinity and surface area can have great influence on an aggregate's reactivity to alkalis. In some aggregates, water molecules may substitute for silica within the framework due to their compatible geometries. This phenomenon effectively weakens the structural integrity of the aggregate, because the new hydrogen bonds (Si-OH$\cdots$OH-Si) are much weaker than the original siloxane bonds (Si-O-Si). Thus, such a substitution tends to make an aggregate more reactive [9].

Over the years, several ASTM standardized tests in conjunction with field experience have made it easier to identify the presence of reactive forms of silica. It has been determined

that only certain forms of silica are notably reactive. Known reactive forms of silica include amorphous silica, quartz, tridymite, cristobalite, opal, chalcedony, and chert [4]. In general, two broad categories of reactive silica can be observed: the crystalline polymorphs of silica such as tridymite and cristobalite as well as the non-crystalline, more disordered forms, which include opals and glasses. The former materials are more reactive than typical quartz because of their low-density frameworks. In both classes of reactive aggregate, the susceptibility to alkali reaction is related to the amount of available sites for hydroxide attack to occur. While a well-crystallized aggregate may not be very reactive (Fig 1.1(a)), a poorly crystalline aggregate (Fig 1.1(b)) has more sites exposed to the attacking hydroxide ions. Thus, the reaction becomes increasingly likely to occur in these aggregates [9].

D. W. Hobbs introduced the concept of a pessimum proportion of aggregate, which is the percentage of reactive aggregate that leads to maximum expansion when exposed to an alkaline environment [1]. If the pessimum proportion is exceeded, the alkalis are so well absorbed by the aggregate that the hydroxide concentration is reduced [10].

1.5 Mechanisms of the Alkali-silica Reaction

To understand the macroscopic effects of the alkali-silica reaction in concrete, it is imperative to understand the micromechanics of the reaction. Thermodynamic and kinetic processes, which ultimately lead to a lowering of the chemical potential of the entire system, control the mechanisms of the reaction on this level. Within the study of ASR, there is much uncertainty and disagreement as to certain aspects of the process, most of this confusion relating to

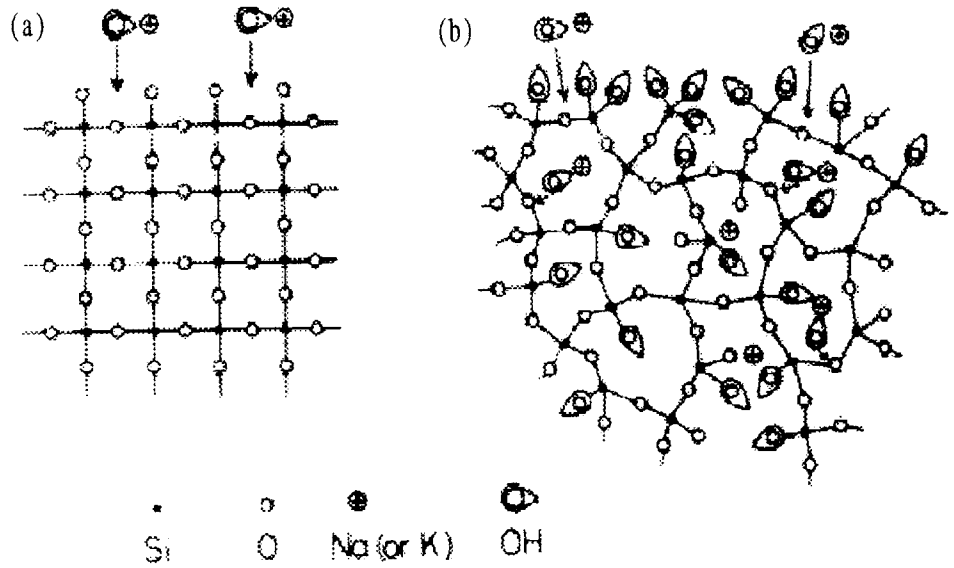

Figure 1.1: Diagrammatic representation of alkali attack (a) on well-crystallized and (b) on poorly crystallized silica [8]

the formation of the deleterious gel. Although a number of theories have been forwarded through the years, it is convenient to place each of these ideas into one of two categories. In the first category, gel formation is modeled as a topochemical process occurring at the aggregate-cement interface; and the second model suggests the possibility of ionic transport through the pore solution with gel formation occurring elsewhere. The two camps disagree in fundamental ways about the chemistry of the reaction as well as the relative importance of the particular ions involved. However, certain points are generally agreed upon [12, 30].

1. The reaction is sensitive to temperature in that its rate is accelerated with temperature increase.

2. The reaction is sensitive to the relative humidity within the concrete. Moisture is essential for the reaction to occur, and the magnitude of (and damage caused by) the reaction increases with the amount of moisture present.

3. The reaction is limited not by the products but by the reactants. This statement is of great importance, because it suggests that as long as reactants are supplied, the reaction will continue regardless of how much gel has been formed.

1.5.1 Attack of the Silicate Network

As described by Chatterji [13] the alkali-silica reaction in portland cement concrete occurs in several stages. The attack of an aggregate's silicate framework is believed to be the first step in this process. Additionally, it is commonly accepted that aggregate attack is initiated by the hydroxyl ions that accompany alkali cations in a highly alkaline solution rather than by the cations themselves. Descriptions of aggregate attack vary somewhat due to the reaction's dependence on pH in forming the products. This stage of the reaction however is clearly topochemical in nature, as it occurs entirely at the interface of the aggregate and alkaline solution [14].

The first requisite of the reaction is a reactive aggregate, having a disordered or poorly crystallized silica network (Fig 1.2(a)). Such an amorphous structure is more open to attack by the hydroxide ions of an alkaline pore solution, which is also essential to the reaction.

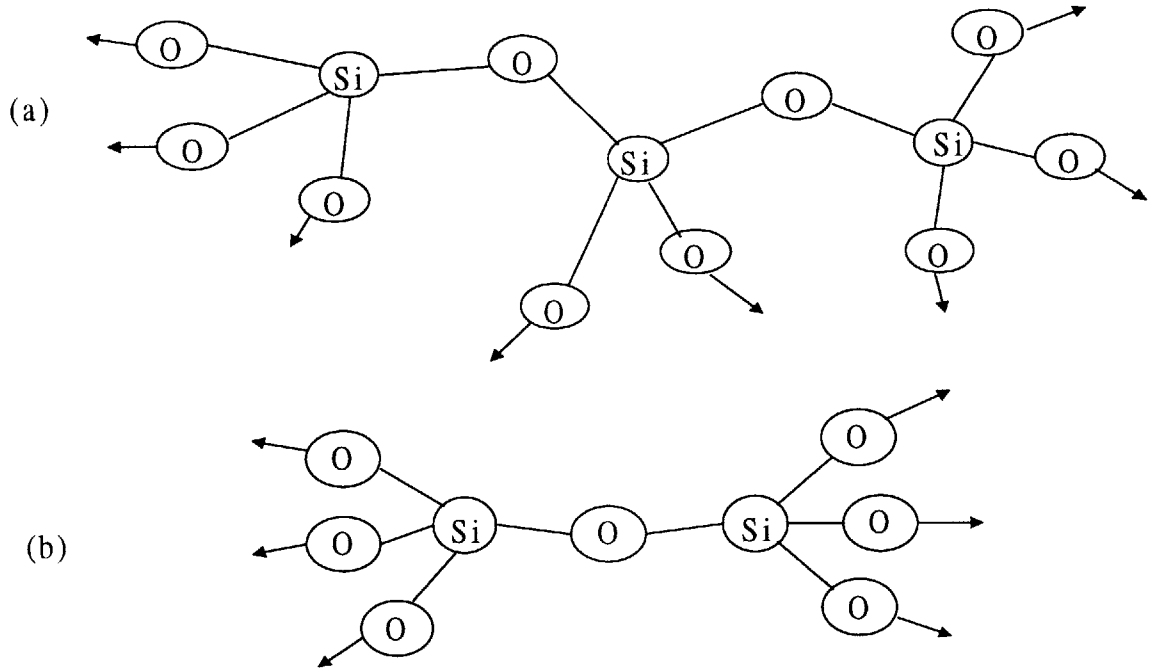

Figure 1.2: Schematic drawing of amorphous silica network. (a) Representative sample of network; b) Simplified version. Note that arrows symbolize siloxane bonds to additional silica atoms, each with three further siloxane bonds, etc.

This framework is conveniently represented by two silica atoms connected to one another by a single oxygen atom, each silica atoms further attached to the network by three siloxane bridges, respectively (Fig 1.2(b)). The six siloxane bonds on the sides form the basis for repetition of the unit, which can be written as →Si-O-Si←. It is assumed that the following process may occur at arbitrary points within the network, given that the siloxane bridges are sufficiently exposed to the alkaline solution.

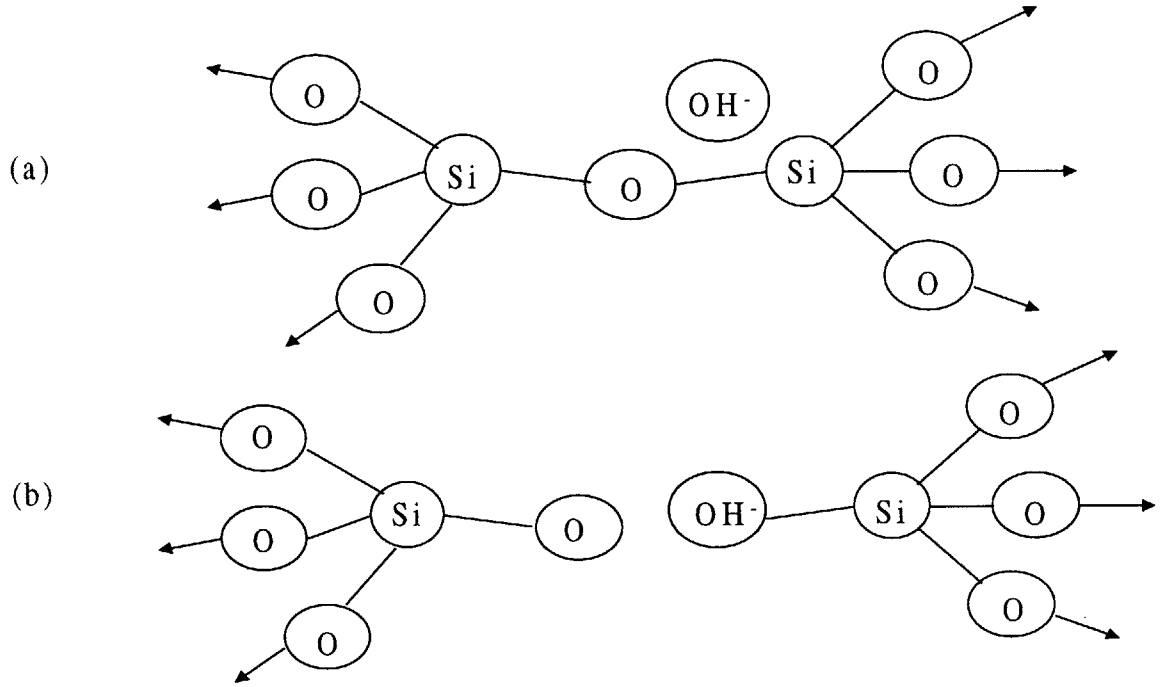

Figure 1.3: Attack of the first siloxane bridge. (a) Approach of hydroxyl ion; (b) Rupture of siloxane bridge and replacement with silanol bridge.

In certain reactive aggregates immersed in pure water, hydroxyl groups, forming →Si-OH silanol bonds, may replace oxygen atoms on the outer surface of the aggregate. This substitution merely has the effect of accelerating the hydroxide attack when exposed to alkaline solution. This effect having been neglected, the first hydroxyl group ruptures one of the siloxane bridges connecting the two silicon atoms (Fig 1.3 (a) and (b)). This hydroxide ion replaces the siloxane bond with a silanol bond, and the unit is essentially split in half.

The process thus far can be represented stoichiometrically as [13]:

$$\rightarrow \text{Si-O-Si} \leftarrow + OH^- \Rightarrow \rightarrow \text{Si-O}^- + \text{OH-Si} \leftarrow \tag{1.1}$$

Negative charges are balanced by the alkaline cations present in solution (Na^+ or K^+). Since both halves are subsequently attacked in a similar fashion, only the right half will be further considered (OH-Si←). Another hydroxide ion may (or may not) react with the silanol bond, replacing the bonded hydroxyl group with a single oxygen atom (Fig 1.4 (a) and (b)).

This reaction is represented by:

$$\text{OH-Si} \leftarrow + OH^- \Rightarrow O^- - S \leftarrow + H_2O \tag{1.2}$$

In essence, this reaction is the same as that which occurs when the hydroxylated surface silica mentioned earlier undergoes hydroxyl attack, except that it would precede the previously given reaction in such cases.

At this point the silica is still attached to the network by three siloxane bridges, and the disintegration of the second and third bridges proceeds in much the same way as the first (Fig 1.5 (a) and (b)).

Assuming that silanol bonds remain following the last two reactions, the breakage of the fourth and last siloxane bond (Fig 1.6 (a) and (b)) culminates in the release of the monomer $SiO_4H_3^-$.

The chemical representation as such is[15]:

$$OH^- + \rightarrow SiO_3H_2^- \Rightarrow SiO_4H_3^- \tag{1.3}$$

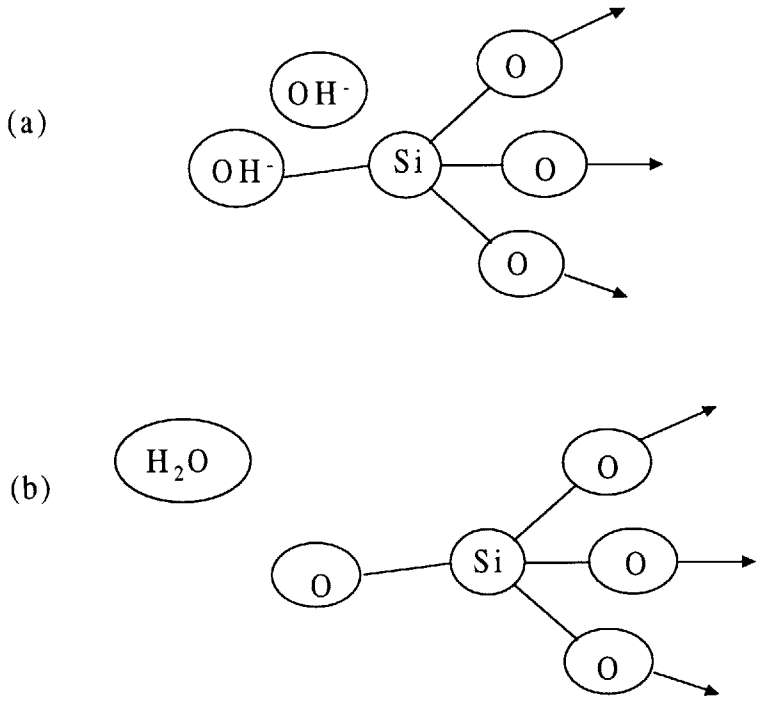

Figure 1.4: Further reaction of ruptured siloxane bond. (a) Approach of hydroxyl ion; (b) Replacement of hydroxyl group with oxygen and release of water.

.

1.5.2 Soluted Monomers

In reality, the monomer that is released depends on how many of the four remaining bonds contain a hydroxyl group, and the number of hydroxyl groups depends in a complex way on the pH of the surrounding solution. Consequently, one must examine the solubility products of the possible species. Dron, Brivot and colleagues [15, 16, 17] have approached this problem by investigating the equilibrium of surface hydrates of silica and the possible soluted

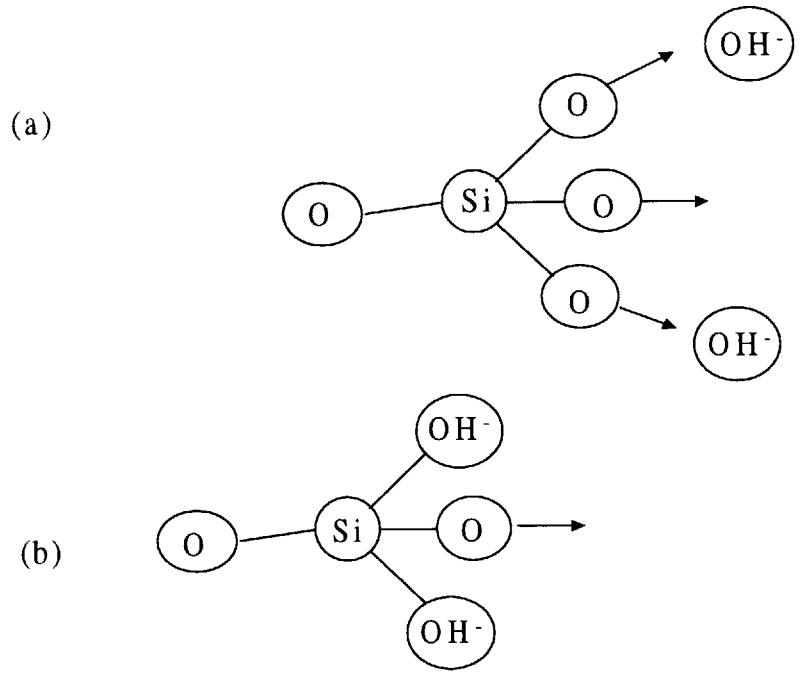

Figure 1.5: Rupture of the second and third siloxane bridges. (a) Approach of hydroxyl ions; (b) Rupture of siloxane bridges and replacement with silanol bridges.

species: SiO_4H_4, $SiO_4H_3^-$, and $SiO_4H_2^{2-}$. Two reactions can be written to characterize the possibilities [18, 19]:

$$SiO_4H_4 \Leftrightarrow SiO_4H_3^- + H^+ \tag{1.4}$$

$$SiO_4H_3^- \Leftrightarrow SiO_4H_2^{2-} + H^+ \tag{1.5}$$

For the first reaction $pK_1 = 9.8$, and for the second $pK_2 = 11.8$. Concentrations of each of the species present can then be determined based on these equilibrium constants:

$$\frac{[SiO_4H_3^-][H^+]}{[SiO_4H_4]} = 10^{-9.8} \tag{1.6}$$

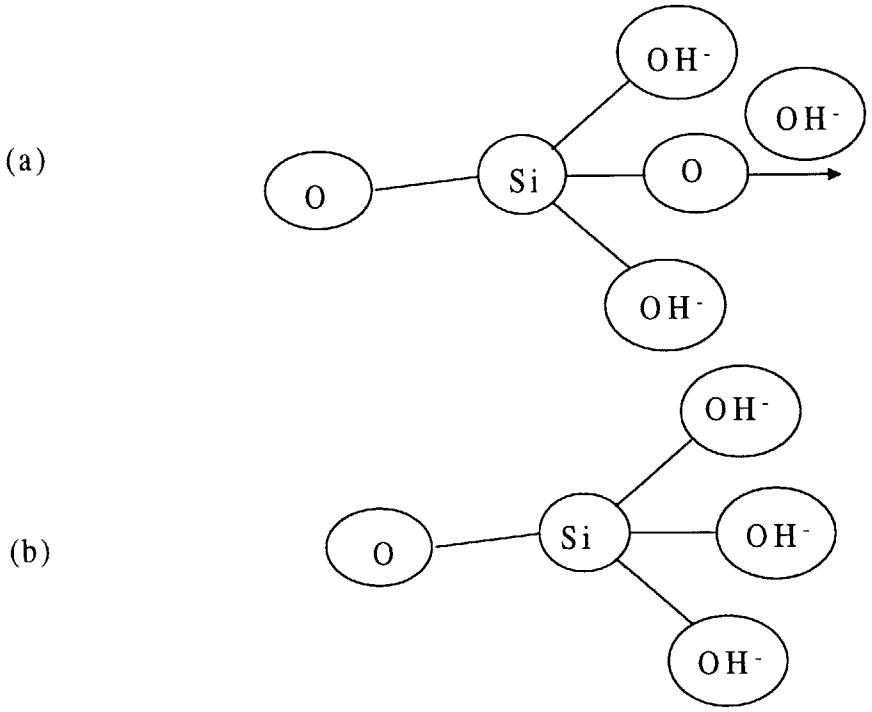

Figure 1.6: Rupture of the last siloxane bridges. (a) Approach of hydroxyl ion; (b) Rupture of siloxane bridges, replacement with silanol bond, and release of monomer.

$$\frac{[SiO_4H_2^{2-}][H^+]}{[SiO_4H_3^-]} = 10^{-11.8} \tag{1.7}$$

Thus, if the pH ($\log[H^+]$) and the concentration of one species are known, the concentration of the remaining species can be easily computed with these equations. Clearly, the concentrations present in solution are dependent on the acidity (or alkalinity) of the solution itself. The reactions detailed above (as well as those described in the previous section) have been simplified for clarity. It should also be noted that the anions in solution are balanced by cations, such as sodium and calcium.

1.5.3 Mechanisms of Gel Formation

Much of the uncertainty mentioned previously relates to the mechanisms by which the deleterious gel is formed within concrete. In the following sections, the main points of the two primary theoretical camps will be investigated. Although even those within a certain camp may disagree, no distinction between mechanisms appears to be more substantial than that between these two schools of thought.

Recently, researchers have begun to agree that calcium ions, Ca^{++}, play an important role in the alkali-silica reaction. The importance of this ion may help explain why evidence of alkali-silica gel has been observed at locations removed from reactive aggregates. Chatterji [13] proposes that the diffusion of silica to other locations is controlled by the concentration of Ca^{++} locally. If the concentration of Ca^{++} is low, the tendency for silica to diffuse is increased, thus implying that the reaction requires the presence of Ca^{++}. These ions (having established in the pore solution equilibrium with Portlandite cystals, $Ca(OH)_2$) may provide the supply of hydroxide that is eventually taken up the alkali ions. West and Sibbick [20] give a simplified example of this type of interaction as follows:

$$Ca(OH)_2 + 2NaCl \Rightarrow 2NaOH + CaCl_2 \tag{1.8}$$

From here, the alkalis apparently begin the hydroxide attack of the silica bonds. The exact nature of calcium's role in ASR is still the subject of debate. However, an understanding of this process may provide the key to determining which of the following mechanisms best describes the reaction.

Topochemical Mechanism

While there is little disagreement that the reaction begins with the topochemical attack of hydroxyl on the siliceous framework of aggregates, the location of the subsequent formation of the deleterious gel is the source of some emerging controversy. The perception that the alkali-silica reaction is primarily topochemical in nature is so common in past research literature that it is practically assumed. Many of the most prominent papers on the subject of ASR have made this assumption that gel formation and expansion always occurs at the aggregate-cement interface [2, 18, 21, 22].

Powers and Steinour [21] describe the surface penetration of the aggregate by the caustic, alkaline pore solution, further noting that this penetration may be visually observed as a "reaction rim". They go on to specify the reaction product as being solid in the absence of water but becoming more fluid with the addition of sufficient water. Following the caustic attack of the siloxane bonds detailed above, molecules are released in solution, possibly in the form of orthosilicic acid, SiO_4H_4. As noted earlier the exact species of monomer is highly dependent on the local pH of the surrounding solution. The molecules freed by the hydroxyl attack then condense to form colloidal particles or a silica sol. Then, the silica sol may condense further, releasing more water and resulting in the formation of new siloxane bonds. Eventually, this ongoing process culminates in the transformation of the silica sol to a silica gel, which is initially weak and brittle but becomes stronger with more siloxane formation.

Even in 1955 [21], it was recognized that calcium ions played some part in the reaction, but excess concentrations of calcium were believed to produce a hard, non-expansive precipitate

(C-S-H) rather than the silica gel [23]. Powers and Steinour have postulated that a zone of this precipitate builds at the surface of silica gel and impedes the diffusion of additional calcium ions into the gel. Such a scenario would lay the groundwork for the osmosis or imbibition theories of expansion to be detailed later. Additionally, this explanation is somewhat similar to the one described in the trans-solution mechanism, although some believers in the topochemical process tend to downplay the importance of calcium.

Trans-solution Mechanism

The trans-solution or through-solution mechanism emphasis the role of the pore solution in the production of the damaging gel. Whereas the topochemical mechanism is controlled in a kinetic sense by the diffusion of the alkali pore solution into the siliceous aggregate, the trans-solution mechanism is controlled by the dissolution of the aggregate into the pore solution [24]. Dron and Brivot are prominent proponents of this theory and have provided a detailed account of the stages of ASR in several papers [15, 16, 17, 25]. The following descriptions will draw heavily from their work.

Released by the alkali attack of the aggregate's silica lattice, the monomer species (e.g. SiO_4H_4, $SiO_4H_3^-$) tend to accumulate at the silica surface forming a transitory "silica gel". This particular gel is not the deleterious gel that forms later but instead is a more soluble, metastable form. The monomers comprising this ionized gel are negatively charged, thus attracting the alkaline cations from the surrounding solution. Because the gel is soluble, the solution becomes locally saturated with monomeric silicate ions and cations. The local state of saturation creates a diffusion gradient between this area and locations of lower ion

concentrations. Thus, the anionic silicate ions and the cationic alkali ions tend to diffuse away from the silica surface.

The other ingredient essential to gel formation is the calcium ion (Ca^{++}), although the significance of this ion is a subject of debate amongst the two mechanistic camps. The film of monomer species that forms at the aggregate surface has been found impenetrable to calcium cations. Clearly, the harmful C-K-S-H (or C-Na-S-H) gel cannot form at this surface if calcium is not allowed into the soluble gel[15]. Furthermore, calcium plays a very important role in determining where exactly the damaging gel will form.

The source of calcium in concrete is the Portlandite crystals, $Ca(OH)_2$, which is obviously a vast resource. However, in highly alkaline solutions the dissolution of portlandite is greatly inhibited due to its solubility product:

For the dissolution reaction:

$$Ca(OH)_2 \Leftrightarrow Ca^{++} + 2OH^- \tag{1.9}$$

$$[Ca^{++}][OH^-]^2 = K_s \tag{1.10}$$

where $K_s = 10^{-4.5}$.

This relationship has the effect of determining the concentration of calcium ions present when portlandite is partially dissociated in solution. Since the solubility product is a constant, an increase in the alkalinity (hydroxyl concentration) of the solution reduces the quantity of calcium ions dissolved in solution (the common ion effect). Thus, in a highly alkaline solution the calcium ion concentration is very low, and locally the solution becomes rapidly saturated. Again, a diffusion gradient is achieved in which calcium ions diffuse into the pore

solutions away from saturated zones.

At this point the monomeric anions, the alkaline cations, and the calcium ions are all transported in solution from their respective saturated sources to lower concentration sinks. When the silicates encounter the calcium, provided the local pore solution is rich in alkaline cations and hydroxyl anions, the insoluble compound C-K-S-H (or C-Na-S-H) precipitates. This compound attracts many of the local ions due to its insolubility and effectively reduces local concentrations of calcium and silicate ions, thus maintaining the diffusion gradient for these ions. The compound rapidly coagulates, becoming a gel. Though gel formation tends to occur near the silica sources, where this formation occurs ultimately depends on the presence and location of calcium.

Should the insoluble gel happen to form between respective ion sources, the gel may act as a semipermeable membrane, limiting (not eliminating) the diffusion of the ions. Consequently, the side of the gel having the lower ionic flow becomes the precipitation front, and the gel continues to build on this side [16].

1.5.4 Mechanisms of Gel Expansion

The reaction of certain forms of silica from aggregates with hydroxide ions from the pore solution culminates in the formation of a gel that induces stresses and subsequently cracking in concrete structures. In a general sense, there exist at least five hypotheses to explain the considerable pressure generated by the gel: simple enlargement, unidirectional pressure, enlargement of the viscous gel by absorption, osmotic cell pressure, and imbibition [26].

These five hypotheses are by no means completely distinct from one another, and certainly, they may not be mutually exclusive.

Simple enlargement assumes the formation of the gel within the aggregate itself, which would preclude the possibility of a trans-solution mechanism. Apparently, this theory supposes that the hydroxyl attack of the aggregate breaks up the siliceous framework to an extent that allows the alkaline pore solution to infiltrate the aggregate and continue the attack within. Again assuming that gel formation occurs at the site of the attack, the gel grows within the aggregate causing the aggregate itself to become enlarged. Given limited space to grow, the aggregate may then induce expansive pressures (and possible cracking) on its surroundings.

According to the unidirectional pressure hypothesis, the gel is damaging primarily in the early stages of its formation when it is still somewhat rigid.[1] At this time the gel is able to exert a unidirectional stress on its surroundings, and, in this way, causes detriment to the concrete. Although a plausible explanation, it seems that the gel, even in the more fluid stages of its development, is capable of exerting pressure over a long period.

Hobbs [1] describes gel enlargement (Fig 1.7) or the absorption theory as a four-stage process resulting in concrete cracking. In the first stage, the gel forms at the aggregate-cement interface, and its growth creates localized internal stresses. Due to the increasing internal stresses, microcracking begins in the second stage of the process. In the third stage the gel, having absorbed so much water, becomes less viscous and flows into the newly formed microcracks. Finally, in the fourth stage the continued expansion of the gel within the

[1] Strictly speaking, the phrase "unidirectional pressure" is a contradiction in terms, as pressure is omnidirectional by definition. Thus, the hypothesis is assumed to refer to a unidirectional stress rather than a pressure.

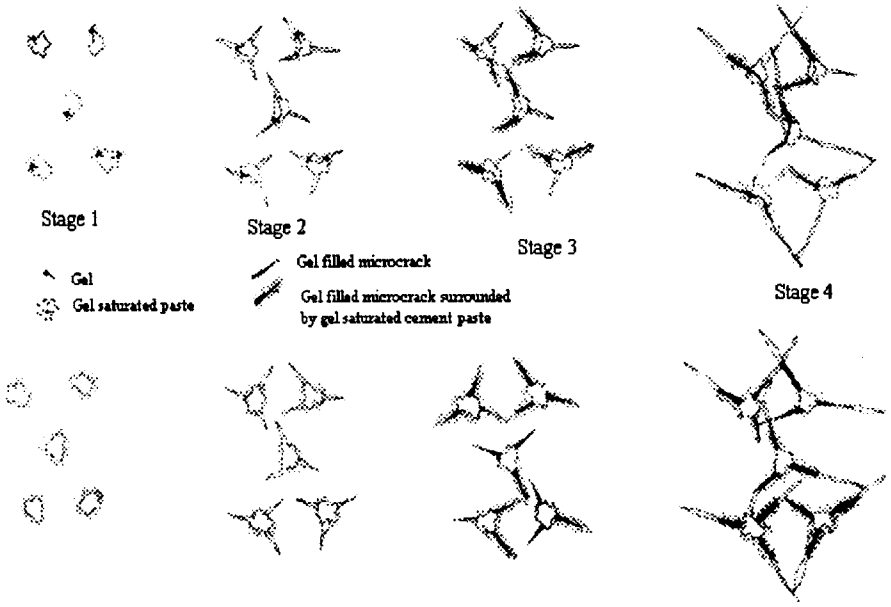

Figure 1.7: Idealization of the absorption theory of gel expansion [1].

microcracks induces more stresses, causing existing cracks to grow and new cracks to form. Whether cracks will form as a result of gel expansion is a function of several variables, such as composition, concentration, and growth rate of the gel.

In the osmotic cell pressure theory, expansion of the alkali-silica gel is related to the difference in chemical potentials inside and outside the gel. According to Diamond [27], the pore solution outside the gel has a higher free energy than that inside, and therefore water flows into the gel.

In a technical sense, osmotic pressure is generated when two solutions of differing ionic

concentration are separated by a semipermeable membrane [21]. Initially it was postulated that cement paste could act as the membrane separating the pore solution from the gel. Critics of the concept have argued that once cracking has begun, the cement is no longer a membrane, yet stresses have been known to increase even after the start of cracking [1]. Regardless of what acts as the membrane, alkalis and hydroxides are permitted to diffuse into the gel while certain silicate reaction products are not allowed to pass through the membrane. In this way, a pressure gradient across the membrane is achieved, inducing the gel to expand [6].

Dent-Glasser has made the point that this process does not occur by osmotic pressure per se, but instead is achieved by imbibition [26]. The mechanism of imbibition is closely related to that of osmotic pressure in that a lowering of free energy in the system drives both. Imbibition, however, need not involve a semipermeable membrane at all. Although cement paste is capable of acting as a membrane, it is not necessary to separate the outside pore solution and the gel, since the gel itself is insoluble. The insolubility of the gel in itself provides the required barrier between the interior of the gel and the solution. Additionally, the liquid of the pore solution is soluble in the gel, and its chemical potential is lowered by this dissolution. That the gel produced in ASR is a polyelectrolyte consisting of negatively charged silicates and alkaline and calcium cations further enhances the imbibition process, since hydration of the charge-bearing gel also lowers the free energy of the liquid.

Even within the frameworks of these theories, there are differing opinions of what actually transpires during the expansion of the gel. The mechanisms described above are simply representative of what is to be found in the literature. In some cases distinctions seem to

be drawn between certain mechanisms by some authors, while others claim that these same methods are virtually synonymous. For example, Diamond [27] speaks of the difference between osmotic and imbibition pressure as being "purely formal".

Chapter 2

Modeling of ASR

The possible micromechanisms of ASR expansion having now been described, the next step in this investigation is the development of a mathematical model that characterizes the observable macroscopic behavior of an ASR-subjected structure. In this chapter, the review of ASR literature continues with the examination of past attempts to model the phenomenon from the perspective mechanics. As will be seen, one of two broad approaches is typically enlisted in these models: either a mesoscopic or a macroscopic framework.

2.1 Introduction

Though the alkali-silica reaction was identified over sixty years ago, little work has been done to generate a numerical model that describes the effects of ASR progression within a struc-

ture. Moreover, the work that has been done has been fairly empirical in its approach. As such, it does not always examine the interaction between the ASR chemical micromechanisms and the material mechanisms that culminate in macroscopically observable deformation. In fact, most modeling of the past has involved the application of imposed thermal loads in some numerical simulation to reproduce structural deformations equivalent to those caused by ASR [28]. Such modeling requires a trial-and-error approach essentially neglecting the relationship between thermochemical conditions and structural behavior. Consequently, this type of approach has met with minimal success.

The history of this past experience exposes the need to develop numerical models that relate observed structural behavior to the physical and chemical factors that influence the course and extent of ASR. The first step in the process of developing such rational models is to examine actual data regarding the reaction. A good way to begin is to first look at the case of unrestrained ASR expansion, that is the case in which ASR expansion is not inhibited by confining stresses or pressures other than those of the concrete skeleton itself. An idealized plot of expansion versus time is s-shaped for the stress-free case (Fig 2.1). The plot consists of three fairly well-developed regimes, which can be identified as periods of initiation, development, and rest [29].

Among the other remarkable observations that can be made of experimental ASR data is the dependence of the reaction on both temperature and water content. Given the overview of the previous chapter, clearly these parameters should enter the formulation of a robust ASR model, as they affect both kinetics and magnitude. It should also be noted that ASR cracking is by definition an irreversible process. That said, the majority of the following models take

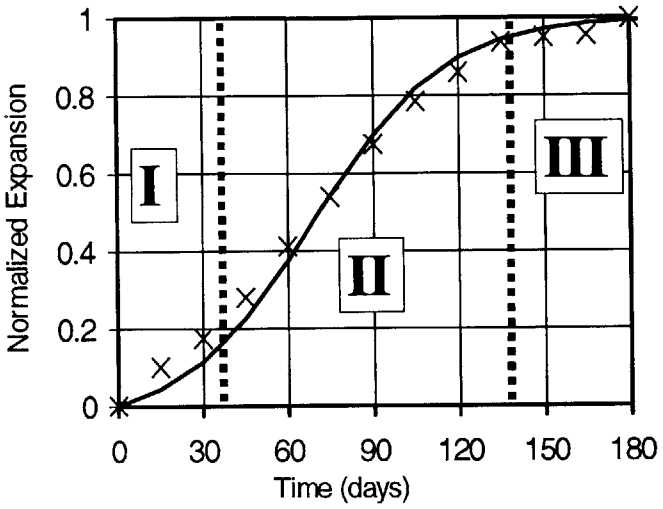

Figure 2.1: A typical plot of stress-free ASR expansion consisting of regions of I) initiation II) development and III) rest

a first order, elastic approach that does not account for macroscopic expansion beyond the elastic regime of the concrete. The last model, however, does extend to a plasticity formulation.

A final aspect of ASR expansion that is not explicitly addressed in any of the models is the issue of stress-induced anisotropy, the effect of uniaxial or biaxial restraint on the volumetric expansion of the gel. This phenomenon was brought to light by Catherine Larive in her PhD test campaign, which shows this anisotropy in dramatic fashion [30]: Whereas pure volumetric expansion is nearly constant for any case of uniaxially applied stress, the strain in the direction of the stress is always reduced, while the strain is increased in the stress-free directions (Fig 2.2). This observation will also be modeled in the next chapter.

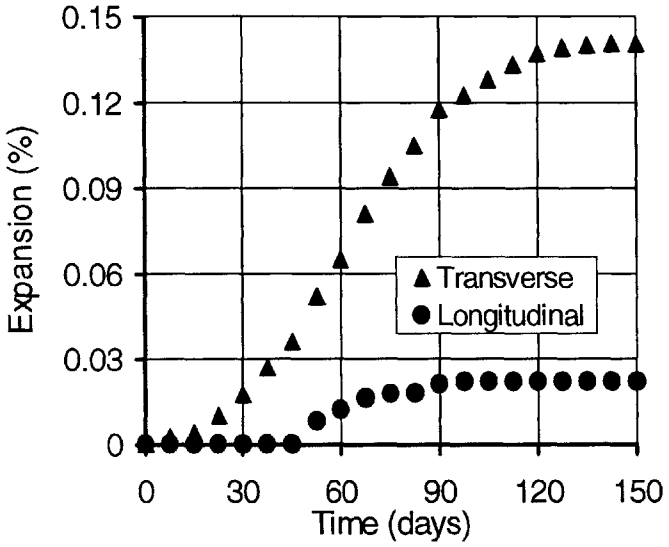

Figure 2.2: Anisotropy of expansion under applied compressive stress[30]

In the following sections a number attempts at mechanism-based modeling that have appeared in recent literature will be examined. The aim in presenting these models is to explore the issues of ASR research previously addressed in the literature, as well as to elucidate the need for coherent, mathematical depictions of both the kinetics and the magnitude of this deleterious phenomenon. For the purposes of this thesis, each of these models has been placed into one of two categories that define the modeling scale: the mesoscopic approach and the macroscopic approach.

2.2 Mesoscopic Approach

The term mesoscopic is used here to describe a modeling approach that examines a material at the largest scale at which it is still recognizable as heterogeneous in composition. The use of this definition implicitly requires that terms such as homogeneous and heterogeneous be defined for the particular application. For the relevant case of ASR and concrete, this scale is the one of the concrete aggregate. Such an approach involves the analysis of a single representative aggregate particle and its immediate surroundings.

2.2.1 Furusawa et al. (1994)

The mesoscopic model presented by Furusawa et al. in 1994 [31] aims to explain the macroscopic expansion of mortar bars by examining first a porous, reactive aggregate exposed to a highly alkaline pore solution. As such, the model emphasizes the dependence of expansion on the diffusion of ions into the aggregate and the ability of the aggregate to accommodate the subsequent increase in volume of the reaction products. To the author's knowledge, this model is the first to employ such a mechanistic approach to the problem of ASR, and it produces fairly accurate values as compared to experimental data.

This mesoscopic model has been developed at the scale of the aggregate. Accordingly, a representative sample of concrete is envisioned to contain many aggregates of some equivalent radius, R_i. The behavior of the concrete on a macroscopic scale is essentially determined by summing the effects of the individual aggregates within. Thus, the model considers only a single aggregate and a small amount of space surrounding it. The qualitative explanation of

the initiation regime of the *s*-shaped curve is that this period represents the time in which the expansion of the ASR reaction product is accommodated by the available aggregate pore space.

Several additional key assumptions have been made in the development of the model that greatly simplify mathematical manipulations:

(1) Since the consumption of hydroxide occurs at a much greater rate than its diffusion, diffusion controls the variation of hydroxide concentration with time.

(2) There exists a porous zone at the periphery of an aggregate that is accommodates reaction products and becomes the reaction product layer.

(3) The capacity of an aggregate to accommodate reaction products is proportional to its surface area.

Clearly, the above assumptions are derived from the larger assumption of a topochemical mechanism, as discussed previously. Most of the following derivation is dependent on this framework. The first assumption was directly employed with Fick's law to obtain the following mass balance from diffusion theory, which gives the variation of hydroxide concentration with time:

$$\frac{\partial C}{\partial t} = \nabla \cdot (D_a \nabla C) + \frac{\partial C_c}{\partial t} \tag{2.1}$$

where D_a is the diffusion coefficient, and $\frac{\partial C_c}{\partial t}$ accounts for the consumption of hydroxides (OH^-) by ASR.

Assuming a uniform and small reacted layer with regard to the size of the aggregate and

assuming the aggregate is comprised completely of reactive silica, the authors then obtained the following relation:

$$\frac{dx}{dt} = k\frac{C_0}{x} \tag{2.2}$$

where x represents the thickness of the reaction layer, k is apparent diffusion coefficient of hydroxide into the aggregate, and C_0 is the hydroxide concentration at the aggregate-cement matrix interface.

The authors additionally found that k depended on temperature through Arrhenius' equation:

$$k = Ae^{-E/(R_g T)} \tag{2.3}$$

where A, E, R_g, and T are the frequency factor, the activation energy, the gas constant, and temperature, respectively. The values of A and E are constants which depend on the particular aggregate and can be determined experimentally. Typical values for these constants are $E = 15$ kcal/mol and $A = 9$ kcal/mol.

If equation (2.2) is integrated, one obtains:

$$x = (2kC_0 t)^{0.5} \tag{2.4}$$

Though the progression from (2.1) to (2.4) is not made more explicit in the literature, it appears that the derivation is that of a 1-D semi-infinite, half-space diffusion problem. Indeed, the well-known, dimensionless solution to this problem closely resembles (2.4). Upon rearranging this equation, the dimensionless Boltzmann variable is obtained:

$$\xi = \frac{x}{\sqrt{2kC_0 t}} \tag{2.5}$$

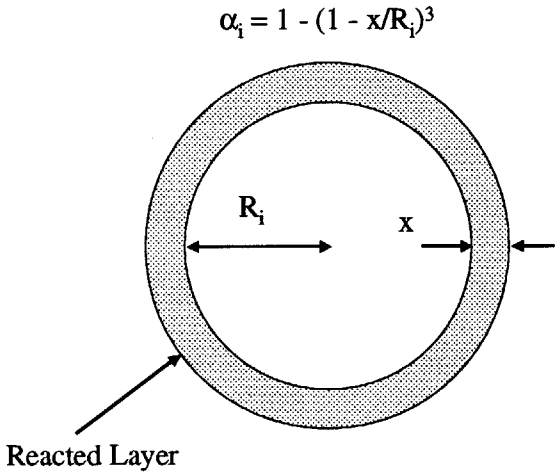

Figure 2.3: Definition of the reaction ratio; after [31]

However, this self-similar aspect of the dissolution process is not pursued by the authors. In return, the progress of the reaction is monitored by the reaction ratio (Fig. 2.3), which is defined as the volume of reacted aggregate per total volume of aggregate of radius R_i:

$$\alpha_i = \frac{R_i^3 - (R_i - x)^3}{R_i^3} = 1 - (1 - x/R)^3 \tag{2.6}$$

The volume of reaction products per volume of concrete can then be obtained:

$$V_t = V_a \Sigma \alpha_i \beta_i \tag{2.7}$$

where V_a is the volume of reactive aggregates per volume of concrete and β_i is the volume fraction of aggregates having an equivalent radius R_i. From this result the molar amount of reaction products per volume of concrete, P_t, can be directly obtained:

$$P_t = V_t \rho_a / \mathcal{M}_{\mathrm{Si}} \tag{2.8}$$

where ρ_a is the specific gravity of the aggregate, and $\mathcal{M}_{\mathrm{Si}}$=60.08 g/mol is the molecular weight of silica.

Next the value of C_0 can finally be obtained:

$$C_0 = (C_{ini} - C_{unit} 3 V_a \Sigma \frac{\beta_i}{R_i} - P_t RS)/W_f \tag{2.9}$$

where C_{unit} is the total amount of hydroxides initially consumed per unit surface of aggregate, RS is the alkali-to-silica ratio of the reaction products, and W_f is the total free water content. C_{ini} is the initial water soluble alkali content, and its value is calculated from the total alkali content and the unit cement content, assuming that 50 percent of the total alkalis are water soluble.

Expansion does not occur until the volume of the porous zone is too small to accommodate the volume of the growing reaction products. This can be expressed by:

$$\varepsilon = B < P_t - P_{abs} > \tag{2.10}$$

where $< x >= \frac{1}{2}(x + |x|)$, ε is the volume expansion, B is an experimentally determined constant, P_t is the amount of reaction product formed, and P_{abs} is the capacity of the porous zone, which is proportional to the overall surface area of the aggregate.

Equations (2.4) through (2.10) give all the relevant parameters for a given time-step. The values of these parameters can be computed with respect to time by repeating the computation iteratively. At $t = 0$, C_0 is set to C_{ini}.

Some important issues of ASR modeling addressed here include the dependence of the reaction on water content and temperature, which both enter the kinetic law given by (2.2).

What appears to be a limitation of the model is that the volume of the reaction products (gel) is assumed to be equal to the volume of the reacted aggregates. Such an assumption does not account for the volume increase of reaction products with respect to the reactants. ASR is generally considered to be a structural problem precisely because volume of the product gel exceeds that of the reactants (i.e. alkali, silica, water). Expansion results from the products requiring more space than is available in adjacent pore space. Without the volume increase, expansion could simply not occur. The model could easily be modified to incorporate this increase in the volume of the reaction products.

This criticism aside, this model does present a logical argument for the description of ASR-kinetics. From a micromechanics perspective, clearly the overriding assumption here is that diffusion controls the progress of the reaction with respect to time. With regard to the magnitude of expansion, the model does not specifically consider such concrete material parameters such as strength and modulus. Instead, these properties are included in the empirical constant, B in (2.10), which is not further developed.

2.2.2 Xi et al. (1999)

The model of Xi et al. (1999) [32] aims at estimating macroscopically observable ASR strain by means of a micromechanics approach operating at the mesoscopic level. In this regard, it extends many of the same concepts addressed in the previous and adds to them. By the same logic employed in the previous model, the kinetics of ASR is assumed to be governed by the diffusion of alkali and hydroxide ion into the aggregate. Additionally, based

on the assumption that gel then migrates from the cement-aggregate interface out into the porous cement matrix, a second process–that of gel permeation–is also modeled. This phenomenon, which controls the growth of the product layer, is described through concepts of fluid mechanics. Finally, these two opposing processes are related and incorporated into a framework of composite theory.

In this model, the cement-aggregate system is envisioned as a composite material that consists of a spherical aggregate center surrounded by a cementitious layer of uniform thickness. With this two-phase system in hand, a simplified equation (which is analogous to that of composite thermal expansion) for the magnitude of macroscopic ASR expansion can be written[1]:

$$\varepsilon = \frac{K_a \varepsilon_a V_a (3K_m + 4G_m)}{K_m(3K_a + 4G_m) - 4V_a G_m(K_m - K_a)} \tag{2.11}$$

where K_a and K_m are the bulk moduli of the aggregates and the concrete matrix, respectively; G_a and G_m are the shear moduli of the aggregates and the concrete matrix, respectively; and ε_a is the expansion of the aggregate. The quantity of interest in equation (2.11) is ε_a, is defined as:

$$\varepsilon_a = \Sigma \phi_i \varepsilon_i \tag{2.12}$$

where ϕ_i is the volume fraction of aggregates with equivalent radius, R_i, and ε_i is the ASR expansive strain of aggregates also of radius, R_i.

To compute ε_i, the two processes of ion diffusion and gel permeation are next considered. First the ion diffusion of alkalis and hydroxides is represented by the mass balance equation

[1]This result is derived from results obtained by Hashin and Shtrikman (1962) who employed variational principles in the computation of bounds for the effective magnetic permeability of multiple-phase homogeneous and isotropic materials [33].

with Fick's law as the conduction law. Similar to (2.1), this mass balance reads:

$$B_{ion}\frac{\partial C}{\partial t} = \nabla \cdot (D_a \nabla C) \tag{2.13}$$

However, in contrast to (2.1), a factor B_{ion} is included to represent the binding capacity of the aggregate. Although a similar form of this equation appeared in the last model, its solution is approached somewhat differently in the present model[2]. Based on the assumption of low aggregate angularity, the aggregate-cement composite is approximated as a perfect sphere, and a spherical coordinate system is employed. This coordinate system eases the analytical solution to the differential equation, which is presented in the form:

$$C(r,t) = C_0 + \frac{2R_i C_0}{\pi r}\sum_{n=0}^{\infty}\frac{(-1)^n}{n}\exp\left(\frac{-\kappa n^2\pi^2 t}{R_i^2}\right)\sin\frac{n\pi r}{R_i} \tag{2.14}$$

where $\kappa = D_a/B_{ion}$. The solution was derived using the following boundary conditions: at $t = 0$, $C = 0$; at $r = R_i$, $C = C_0$; and $C = 0$ at $r = 0$.

The minimum hydroxide concentration required for ASR to occur can be determined experimentally, and this value is then used in (2.14) to solve for the radial distance from the center of the sphere at which ASR is first initiated. Subsequently, the depth of ASR, $x = R_i - r$, is computed.

In second step, a quantity similar to the reaction ratio of the previous model, the reacted volume of aggregate, V_{Ri}, is calculated. With ASR depth x, V_{Ri} is obtained from the spherical geometry in the form:

$$V_{Ri} = \left[\frac{R_i^3 - (R_i - x)^3}{R_i^3}\right]\left(\frac{4}{3}\pi R_i^3\right) = \left[1 - \left(1 - \frac{x}{R_i}\right)^3\right]\left(\frac{4}{3}\pi R_i^3\right) \tag{2.15}$$

[2]Equation (2.13) can be derived from (2.1) by assuming an equilibrium relation between C_c and C, i.e. $C_c = C_c(C)$. Then, $B_{ion} = 1 + \frac{\partial C_c}{\partial C}$ accounts for the binding capacity, which controls the variation for free hydroxide ions.

Since the total reacted volume of one aggregate has now been found, the formula is extended to the rest of aggregates in the form:

$$V_R = V_a \phi_i V_{Ri} \tag{2.16}$$

Finally, the total volume of gel produced is found by a ratio relating gel volume to total reacted aggregate volume:

$$V_{gel} = \eta V_R \tag{2.17}$$

where $\eta > 1$ is the reacted aggregate volume; this ratio η may depend on age t, but this dependency is not explicitly given.

The volume of gel having now been established, the gel permeation aspect of the model can be presented. Essentially, a fluid mechanics argument is employed to this end, considering the gel to be a viscous fluid forced into the cement paste pores by building pressure within the aggregate. Accordingly, the gel permeation of the viscous gel is described by Darcy's law:

$$\frac{\partial C_{gel}}{\partial t} = \nabla \cdot \left[\frac{\kappa_{gel}}{\eta_{gel}} \nabla P \right] \tag{2.18}$$

where C_{gel} is the concentration of gel in the cement pore, η_{gel} is the gel's viscosity, κ_{gel} is the permeability of the cement paste to the gel, and P is the pressure generated at the cement-aggregate interface. The solution to this differential equation is complicated by coupling between C_{gel} and P. Thus, these parameters, as well as temperature T, are now related by an equation derived in ASTM C1260. For a constant temperature (80°C), this equation is expressed as follows:

$$C_{gel} = \frac{C_p}{f_t} P \tag{2.19}$$

where C_p is the porosity of the interfacial cement paste, and f_t is the tensile strength of the paste. This form is obtained by the assumption that the gel has saturated the pores of the cement paste, giving $C_{gel} = C_P$. Finally, equation (2.18) is solved with the aid of three boundary conditions. Initially $(t = 0)$, $c_{gel} = 0$. For any time t, $C_{gel} = \frac{C_p}{f_t} P(t)$ at the cement-aggregate interface, and $C_{gel} \cong 0$ at the average half-distance between two aggregates, R_{if}. With these initial boundary conditions and (2.19) in hand, the analytical solution of (2.18) is obtained:

$$C_{gel}(r,t) = \frac{2\beta}{r\,(R_{if} - R_i)} \sum_{n=0}^{\infty} \exp\left[\frac{-\nu n^2 \pi^2 t}{(R_i - R_{if})^2}\right] \sin\left[\frac{n\pi(r - R_i)}{(R_{if} - R_i)}\right] \left(\frac{-n\nu\pi R_i}{(R_i - R_{if}} \int_0^1 \exp\left[\frac{\nu n^2 \pi^2 \lambda}{(R_i - R_{if})^2} P(\lambda) d\lambda\right]\right) \tag{2.20}$$

where $\nu = K_{gel}/\eta_{gel}$. This equation is also coupled due to the dependence of P on time and must be solved numerically.

Lastly, the total volume of surrounding an average-sized aggregate at any time t is given by:

$$V_{pgi} = \int_{R_i}^{R_{if}} 4\pi r^2 C_{gel} dr \tag{2.21}$$

and the total volume of gel absorbed in the pore of the aggregate is:

$$V_{pg} = V_a \phi_i V_{pgi} \tag{2.22}$$

The expansive strain resulting form one aggregate can be expressed directly:

$$\varepsilon_i = \frac{< V_{gel} - V_{pg} >}{\phi_i V_a} \tag{2.23}$$

where $< x >= \frac{1}{2}(x + |x|)$. Essentially, the numerator of this equation expresses that volumetric expansion results when the aggregate pore space can no longer accommodate the growing gel.

Whereas it was not apparent in the model of Furusawa at al. (1994), the increase in volume resulting from gel formation is made clear in this model. Here the treatment of ASR kinetics is similar to that of the previous model, the notion of diffusion controlling the reaction again providing the key assumption. Under the apparent additional assumption of complete water saturation and constant temperature, absent here is any description of reaction dependence on water content and temperature. The model of gel permeation introduced here also suggests the perspective that the gel is fluid-like as it moves from the aggregate out into the cement pore space.

2.2.3 Bažant and Steffens (1999)

This last mesoscopic ASR model [14] aims to describe the kinetics underlying observable ASR expansion without examining the structural effects of the reaction. As in the previous two models, the aggregates are assumed to be perfectly spherical and composed entirely of reactive silica. Rather than examining a single aggregate embedded in an infinite medium of cement, this model considers a representative cube of concrete containing one spherical aggregate (Fig 2.4).

For the representative cube, the following relation holds concerning the mass of the silica:

$$s^3 \xi_s = \varrho_s \frac{\pi D^3}{6} \tag{2.24}$$

where ξ_s is the mass of reactive silica per unit volume of concrete (kg/m^3) and ϱ_s is the mass density of reactive silica (kg/m^3); D and s are the length dimensions of the model (Fig. 2.4). As with the previous models, it is assumed here that the rate of diffusion through the gel

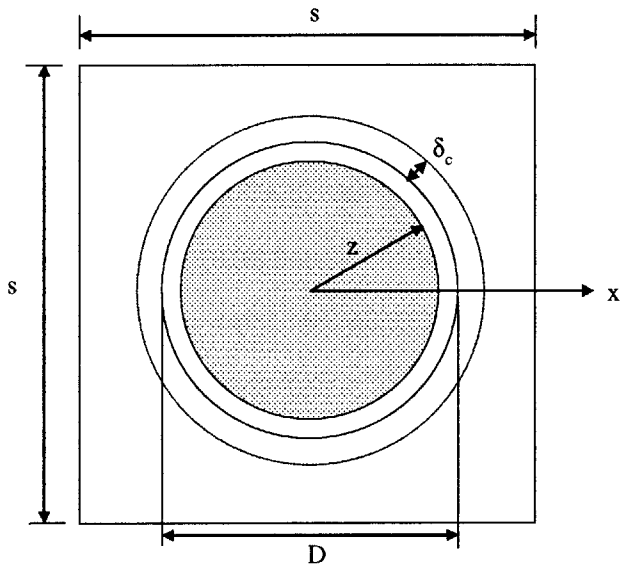

Figure 2.4: Representative cube containing a single aggregate; after [14]

product into the aggregate is very slow compared to the rate of silica consumption at the aggregate surface. Hence, a relation governing the diffusion is required, and again Fick's law is used to this end. This model clearly distinguishes between the formation of gel and its subsequent expansion through the uptake of water. It is noted that the mere production of the gel is not an expansive process in itself. Thus, the first part of the derivation leads to the mass of gel produced per volume of concrete before expansion occurs.

Because the topochemical attack of the reactive silica is essentially immediate, it is postulated that the formation of a gel layer around the aggregate is nearly instaneous. It follows that further reaction is hindered by the gel layer surrounding the aggregate, and the alkaline pore solution must diffuse through this (growing) layer. The shape of the gel layer is approximated

as a spherical shell, and the radial flux of solution into the gel is given by Fick's law:

$$\mathrm{w}_w = -a_s \nabla \xi_w \tag{2.25}$$

where w_w is the flux vector of water out of a given volume Ω containing the reaction front, a_s is the permeability (treated here as an apparent diffusivity coefficient by the authors) of the gel to water in (m^2/s) and ξ_w is the water concentration of the gel, which varies radially. Mass conservation dictates that:

$$\frac{\partial \xi_w}{\partial t} + \nabla \cdot \mathrm{w}_w = 0 \tag{2.26}$$

Combining the two equations and assuming constant permeability gives:

$$\frac{\partial \xi_w}{\partial t} - a_s \nabla^2 \xi_w = 0 \tag{2.27}$$

As a consequence of the slow diffusion of solution through the gel, the radial profile of ξ_w is assumed to be of a steady state. Thus, the following Poisson differential equation holds for spherical coordinates:

$$\nabla^2 \xi_w = \frac{\partial}{\partial x}\left[\frac{1}{x^2}\frac{\partial}{\partial x}(x^2 \xi_w)\right] = 0 \tag{2.28}$$

Integrating (2.28) gives:

$$\xi_w = wF\left(\frac{x}{D}\right) \tag{2.29}$$

where w is pore water concentration outside of gel layer (kg/m^3) and:

$$F\left(\frac{x}{D}\right) = \frac{12(x/D)^4 - 16(x/D)^3(z/D) + 16(z/D)^4}{3(x/D)^2 - 8(x/D)^2(z/D) + 16(x/D)^2(z/D)^4} \left(\frac{z}{D} \leq \frac{x}{D} \leq \frac{1}{2}\right) \tag{2.30}$$

As can be seen in (Fig 2.2), x represents the radial coordinate of the spherical reference system, and $x = z$ gives the position of the reaction front. Next, the authors implicitly invoke the Rankine-Hugoniot condition of mass balance for water at the surface of discontinuity

existing at the reaction front; this conditions reads:

$$[\mathrm{w}_w - r\rho_s \mathrm{V}] \cdot \mathrm{n} = 0 \tag{2.31}$$

where $r\varrho_s$ is the amount of water present at the reaction front, r is the stoichiometric conversion ratio specifying the fraction of moles of water to moles of silica, ϱ_s is mass density of reactive silica, and $\mathbf{V}$ is the velocity of the front in the normal direction $\mathbf{n}$. Indeed, substitution of Fick's law (2.25) across the discontinuity into the Rankine-Hugoniot formulation (2.31) gives the jump condition at the discontinuity surface, presented by the authors in the form:

$$r\varrho_s \frac{dz}{dt} + a_s \frac{\partial \xi_w}{\partial x} = 0 \tag{2.32}$$

Now solving for the rate of reaction front movement and plugging (2.29) into (2.32) gives:

$$\frac{dz}{dt} = -\frac{2a_s}{r\varrho_s D}\left[\frac{\partial}{\partial x} F\left(\frac{x}{D}\right)\right]_{x=z} \tag{2.33}$$

Assuming a mole of pre-swelling gel formed per mole of silica dissolved, the mass of pre-swelling gel is given by:

$$\xi_g = \frac{4\pi}{3}\left(\frac{D^3}{8} - z^3\right)\varrho_s \frac{m_g}{m_s}\frac{1}{s^3} \tag{2.34}$$

where m_g is the molar mass of gel, and m_s is the molar mass of silica. The gel becomes expansive through the imbibition of water and can be accommodated to a certain extent by space in the vicinity of the aggregate. In addition to the capillary pore space within adjacent cement paste, there is a highly porous interstitial layer of cement around the aggregate that can contain gel. Any amount of gel beyond the capacity of this space will induce stresses in the surrounding cement paste. This model focuses on the swelling kinetics without considering the effects of expansion on the surrounding concrete matrix. The growth of the

gel is assumed here to be independent of its initial formation and to occur only through the imbibition of water. The form of this volumetric growth is given as:

$$tr(\varepsilon_g) = \frac{w_i}{\varrho_w} \tag{2.35}$$

where $tr(\varepsilon_g)$ is the volumetric strain of the gel, w_i is the mass of water imbibed by the gel, and ϱ_w is the density of water. In other words, the volume increase of the gel is equal only to the volume of the water imbibed. The evolution of the imbibition process is described in a discrete micro-diffusion rate equation:

$$\dot{w}_i = \frac{H_0}{\tau_i} A_i \tag{2.36}$$

where A_i is the reaction affinity, τ_i is the imbibition halftime, a time constant that reflects the ability of the porous layer to accommodate water, and H_0 is a constant that represents the fact that the thickness of the interstitial layer around the aggregate cannot exceed the space available in the representative cube.

Based on a set of simplifying assumptions, which will not be detailed here, an approximate form for the affinity is developed:

$$A_i = n(p)m(p)\xi_g - w_i \tag{2.37}$$

where the empirical functions $m(p)$ and $n(h)$ represent the dependence of the affinity on the internal pressure of the gel and the relative pore humidity, respectively.

The solution of equation (2.36), which can be integrated numerically, yields the solution to equation (2.35), which gives the volume increase of the gel. Again, the goal of this model is a mathematical description of the kinetics of ASR, not the structural consequences of

the expansion. Some of the theory behind the model extends the work presented in the previous two models, particularly the assumptions about diffusion. However, some new ground covered here would include the distinction between gel formation and expansion, as well as the introduction of thermodynamic affinity. Additionally, it should be noted that the temperature dependence of the reaction is not explicitly addressed here. However, its inclusion should be straightforward, as the model employs elementary notions of fluid properties.

2.3 Macroscopic Approach

The term macroscopic is used here to describe a modeling approach that examines materials at the scale of a representative volumetric element [34]. The element is representative in that it should have properties similar, in an a average sense, to those of any other like-sized element taken from elsewhere in the structure. The approach is that employed in continuum mechanics, and it can be more tangibly illustrated by a comparison of typical dimensions of some characteristic structure. For a Civil Engineering structure, typical dimensions might consist of B, W, and H, for the base, width, and height of the structure, respectively. Keeping in mind the level of governing heterogeneity defined as mesoscopic previously, the dimensions of a representative volume can be chosen. To illustrate, if the volumetric element is selected as a cube of side, l, and the average size of aggregate is D (mesoscopic dimension), the following should hold true:

$$D \ll l \ll B, W, H$$

Once one element has been identified, part or all of the structure can be envisioned as being composed of identical representative elements. If, for the case of ASR, D is considered the aggregate size, then l defines the typical scale of laboratory test specimens (e.g. cylinder ϕ16 cm) , which–in general–is much smaller than the size of structural elements, B, W, and H. Since the model accounts for the behavior of one element, the addition of other elements allows the prediction of the behavior of the whole structure.

2.3.1 Chatterji and Christensen (1990)

The following model [36] attempts to predict the observable expansion of mortar prisms due to ASR. Presumably, this work with mortar prisms is extendable to larger scale concrete structures, although there is clearly a difference in the size of aggregates. In this sense, the model does not strictly fit into the category of macroscopic modeling as defined here. However, since the dimensions of the mortar prism are much larger than the diameter of an average aggregate particles, this model can be considered macroscopic as previously defined. Because only small aggregates (sand particles) are used in mortar, it should be remembered that the prism is not a representative elementary volume as such, but rather a scaled-down version of a larger structure.

Unlike the previously examined models, this one is concerned with the ultimate expansion due to ASR, not its variation with time. Here, time dependence is not considered, except insofar as it pertains to the maximum expansion. The equation for expansion was attained first through the identification of the relevant parameters, namely the alkali concentration, C,

and the temperature, θ. Expansion data were then obtained for various value of C and θ and for a number of different sands. Equations were then fit to the data sets using least-square methods. The equations had the following form:

$$\varepsilon = SK[1 - M < C - C_0 > -N(\theta - \theta_0) + P < C - C_0 >< \theta - \theta_0 >] \tag{2.38}$$

where $< x >= \frac{1}{2}(x + |x|)$, and the "0" subscripts indicate threshold values below which expansion is believed not to occur. S and K are experimentally determined constants that apparently have some dependence on the type of sand used in the mortar. Further dependence of these constants is not explored. The constants M, N, and P are also experimentally determined. Another form of equation (2.38) is presented that assigns physical meaning to some of these constants:

$$\varepsilon = SK[1 - \frac{\partial \varepsilon}{\partial C}\Delta C - \frac{\partial \varepsilon}{\partial \theta}\Delta\theta + \frac{\partial^2 \varepsilon}{\partial C \partial \theta}\Delta C \Delta\theta)] \tag{2.39}$$

in which the Δ operator indicates a change in the parameter that follows it. The validity of this relation is not pursued in the literature, and its derivation is unclear. Accordingly, the model is treated here as an equation fit to data with many experimental constants of unknown dependencies. Additionally, the variation of expansion with time is not investigated, which likely is a crucial point in any enduring mechanistic model. However, this line of research might be useful if more were discovered about what the various terms represent in a physical sense and of what parameters they are functions.

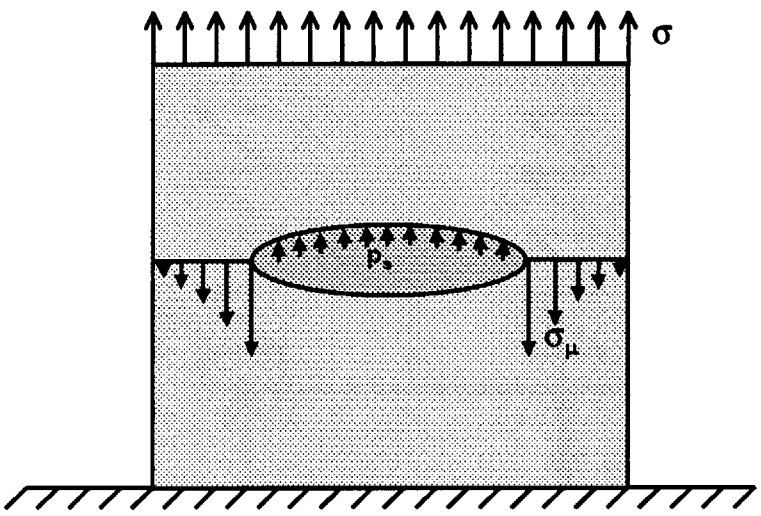

Figure 2.5: Mesoscopic mechanism for ASR expansion [34]

2.3.2 Coussy (1995)–Larive (1998)–Ulm et al. (2000): Chemoelasticity

The chemoelastcity model [24, 30, 34] of ASR expansion predicts the macroscopic behavior of ASR-subjected concrete by considering the underlying chemical micromechanisms involved in the reaction. It is based on Coussy's theory of reaction in porous media [35]. In this first approximation of material behavior, the expansion of the gel is assumed to elicit an elastic response by the surrounding concrete. Furthermore, this model addresses the chemical evolution of ASR, as well as incorporates the effect of an externally applied load. To elucidate all the mechanisms at work, a simple 1-D rheological representation is employed, consisting of a pressure cell and elastic springs. In the extension to three dimensions, a thermodynamic argument is invoked in which the energy state and dissipation of the system are examined.

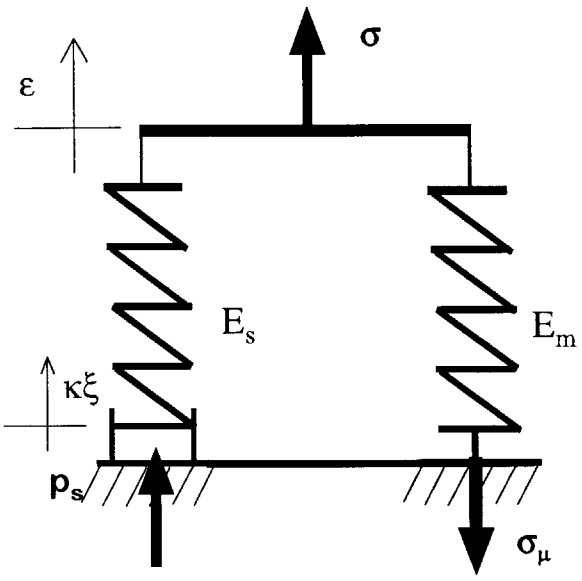

Figure 2.6: Rheological representation of chemoelasticity [34]

1-D Chemoelasticity

The problem of ASR expansion can be envisioned as a concrete sample containing a gel-filled void that exerts pressure on the surrounding concrete matrix. In turn, the concrete skeleton resists this pressure with tensile stress. This mesoscopic system, including an externally applied load, is sketched in Figure 2.5. For the purposes of understanding and modeling, a 1-D think model (Fig. 2.6) is developed to represent the relevant aspects of ASR expansion. In this device, E_s and E_m are elastic stiffnesses, ε is the overall strain of the system, p_s is the swelling pressure exerted by the gel, σ_μ is the resisting stress provided by the concrete skeleton, and σ is the externally applied stress. The expansive strain of the gel itself is represented by $\kappa\xi$, in which κ is a dilatation coefficient that quantifies the gel growth with respect to the reaction extent, $\xi \in [0,1]$. The reaction extent measures the progress of the

reaction, $\xi = 0$ indicating the beginning of the reaction, and $\xi = 1$ representing the completion of the reaction. Within this quantity is expressed the underlying chemistry of the model, which will be later detailed.

From the rheological scheme, equations describing the stress equilibrium of the system are readily obtained. The externally applied load must be balanced by the difference between the restraining stress of the concrete skeleton and the swelling pressure of the gel:

$$\sigma = \sigma_\mu - p_s \tag{2.40}$$

This equation can be further advanced by noting that $\sigma_\mu = E_m\varepsilon$ and $p_s = E_s(\kappa\xi - \varepsilon)$:

$$\sigma = E_m\varepsilon + E_s(\varepsilon - \kappa\xi) \tag{2.41}$$

Now, the case stress-free expansion ($\sigma = 0$) is considered in order to establish a parameter called the chemical dilatation coefficient, β:

$$\varepsilon = \frac{E_s\kappa}{E_m + E_s}\xi = \beta\xi; \qquad \beta = \frac{E_s\kappa}{E_m + E_s} \tag{2.42}$$

The chemical dilatation coefficient relates the progress of the reaction directly to the observable strain. As might be inferred, this coefficient is a function of the total stiffness of the concrete and the intrinsic chemical dilatation of the gel, κ. All that is needed now in this formulation is a quantitative description for the evolution of the chemical reaction. The form of this evolution can be determined from the difference in chemical potentials of the reactants, the affinity.

From thermodynamics, the affinity, $A_m = A_m(\xi)$, constitutes the driving force of a chemical reaction. The reaction proceeds when the affinity has a non-zero value, beginning with some

initial value, A_{m0}. As the affinity approaches zero, the reaction approaches completion. Thus, for $A_m = A_{m0}$, $\xi = 0$, and for $A_m = 0$, $\xi = 1$. Identification of the affinity of the driving force of the affinity as the driving force of the reaction immediately allows for the formulation of the reaction's kinetic law:

$$\dot{\xi} = \frac{d\xi}{dt} = F(A_m) \tag{2.43}$$

Assuming a linear kinetic law for the stress-free case ($\sigma = 0$):

$$k_d \frac{d\xi}{dt} = A_m(\xi); \quad k_d > 0 \tag{2.44}$$

where k_d is a chemical kinetic coefficient. Lastly, for this case, a time constant, $t_c = k_d/A_{m0}$, is defined such that (2.44) becomes:

$$1 - \xi = t_c \frac{d\xi}{dt} \tag{2.45}$$

At this point, the kinetic law has been developed for the case of stress-free expansion; however the thermodynamic argument of the next section will show the validity of the law for all stress cases. The time constant, t_c, depends on temperature and reaction extent the following experimentally determined way [30]:

$$t_c = \tau_c(\theta_0) \frac{1 + \exp[-\tau_L(\theta_0)/\tau_c(\theta_0]}{\xi + \exp[-t/\tau_c + \tau_L/\tau_c]} \tag{2.46}$$

where the time constants τ_L and τ_c are the latency time and the characteristic time, respectively, while θ is the temperature. τ_L is associated with the dissolution of silica from the aggregate, while τ_c is associated with the mechanism of gel formation. Integration of the kinetics law (2.45) with (2.39) yields the reaction extent directly:

$$\xi(t) = \frac{1 - \exp(-t/\tau_c)}{1 + \exp(-t/\tau_c + \tau_L/\tau_c)} \tag{2.47}$$

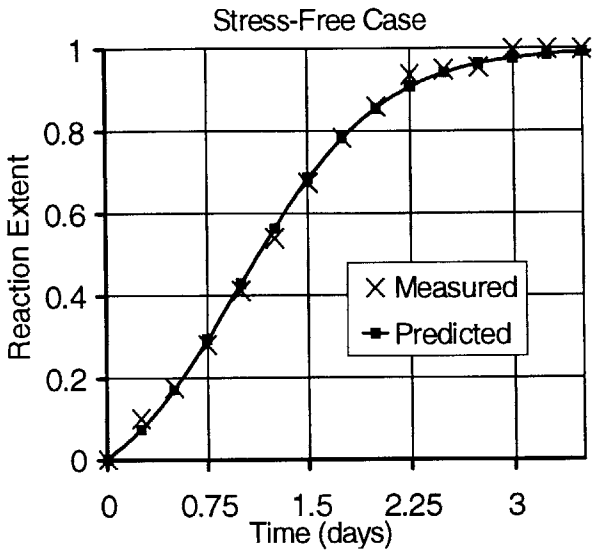

Figure 2.7: Predicted and measured reaction kinetics

With the above formulation and the assumption that $\tau_L/\tau_c = 3$, a plot (Fig. 2.7) of reaction extent as a function of normalized time can be produced and compared with actual test data.

From the plot it can be seen that this model produces as s-shaped curve that matches the test data very closely. A more in-depth description of the process of generating the predicted expansion curve follows in Chapter 3.

1-D Chemoelasticity: Energy Considerations

Approaching the same problem from the perspective of thermodynamics offers a robust view of the chemoelastic model, which is employed for the extension of the 1-D model to

three dimensions. The first step of the derivation involves application of the First Law of Thermodynamics. This law states that the variation of the system's internal energy, dU, is the incremental sum of external work, $dW = \sigma d\varepsilon$, and the externally supplied heat, $Q^{\circ}dt$:

$$dU = \sigma d\varepsilon + Q^{\circ}dt \tag{2.48}$$

To supplement the information provided by the First Law, the Second Law of Thermodynamics is applied. This law states that the variation of internal entropy, dS, of a homogeneous system must always equal or exceed the entropy externally supplied by heat, $\left(\frac{Q}{\theta}\right)^{\circ} dt$:

$$dS \geq \left(\frac{Q}{\theta}\right)^{\circ} dt \tag{2.49}$$

where θ is the absolute temperature. The Second Law expresses whether or not the energy put into a system can be recovered. For instance, if $dS = \left(\frac{Q}{\theta}\right)^{\circ} dt$ all the energy supplied to the system is subsequently recoverable, while if $dS > \left(\frac{Q}{\theta}\right)^{\circ} dt$, some energy is lost due to dissipation, the irreversible transformation of useful work into heat. The evolution of dissipation over time, dt, can be determined by combining and rearranging (2.48) and (2.49):

$$\varphi dt = \sigma d\varepsilon - (dU - \theta dS) \geq 0 \tag{2.50}$$

This expression can be made yet more useful through the introduction of the Helmholtz energy (or free energy), ψ, a measure of the maximum capacity of a system to do work:

$$\psi = U - \theta S \tag{2.51}$$

the differential of which is under isothermal conditions (i.e $d\theta = 0$):

$$d\psi = dU - \theta dS \tag{2.52}$$

Substitution into (2.50) gives the Clausius-Duhem inequality:

$$\varphi dt = \sigma d\varepsilon - d\psi \geq 0 \tag{2.53}$$

From the rheological scheme developed in the previous section, the Helmholtz energy can be expressed as:

$$\psi = \frac{1}{2}[E_m\varepsilon^2 + E_s(\varepsilon - \kappa\xi)^2)] + g(\xi) \tag{2.54}$$

where $g(\xi)$ is the free energy of the pressure cell. In incremental form, (2.54) becomes:

$$d\psi = [E_m\varepsilon + E_s(\varepsilon - \kappa\xi)]d\varepsilon + g(\xi) + [-E_s(\varepsilon - \kappa\xi)\kappa + \frac{\partial g}{\partial \xi}]d\xi \tag{2.55}$$

With (2.55), (2.53) consequently is written:

$$\varphi dt = [\sigma - (E_m\varepsilon + E_s(\varepsilon - \kappa\xi))]d\varepsilon - \left[\kappa E_s(\varepsilon - \kappa\xi) - \frac{\partial g}{\partial \xi}\right] d\xi \geq 0 \tag{2.56}$$

A comparison of (2.41) and (2.56) reveals that:

$$\sigma = \frac{\partial \psi}{\partial \varepsilon} = E_m\varepsilon + E_s(\varepsilon - \kappa\xi) \tag{2.57}$$

From this relationship, the driving force of the reaction can be identified as:

$$A_m = -\frac{\partial \psi}{\partial \xi} = -\kappa E_s(\varepsilon - \kappa\xi) - \frac{\partial g}{\partial \xi} = -\kappa p_s - \frac{\partial g}{\partial \xi} \tag{2.58}$$

and the dissipation can be expressed as:

$$\varphi dt = \left[-\kappa p_s - \frac{\partial g}{\partial \xi}\right] d\xi = A_m d\xi \geq 0 \tag{2.59}$$

For this dissipation, it turns out that the energy consumed in the chemical reaction, $\frac{\partial g}{\partial \xi}d\xi$, is much larger than the energy supplied by the pressure, $-p_s\kappa\xi$. Thus, this term can be neglected in the computation of the dissipation, as well as for the affinity:

$$A_m = -\frac{\partial g}{\partial \xi} \tag{2.60}$$

the linear form of which would be:

$$A_m = A_{m0}(1 - \xi) = k_d\frac{d\xi}{dt} \tag{2.61}$$

This equation corresponds to the kinetic law developed in the previous section for the 1-D case. However, the preceding derivation was not limited to a particular load case, and thus the relation holds for any load, σ. The approach described above will be applied in Chapter 3 to the case of chemoplasticity.

2.3.3 Huang and Pietruszczak (1999)

The following macroscopic scale ASR model was first presented in 1996 [37] to describe the macroscopic expansion and subsequent degradation of ASR-subjected structures. The model was later refined in several other papers [38, 39]. In this model, the time evolution of macroscopic strain is initially defined mathematically for the elastic regime of deformation. The key parameters affecting the reaction are identified and incorporated into this mathematical formulation. Special attention is given to the influence of temperature on the reaction kinetics. To this end, it is postulated that below a certain threshold temperature the progress of ASR is very slow. This idea is expressed in the thermal activation time, a function that relates time and temperature. Following the development of an elastic expression for the expansive strain, the model is extended to include plastic effects through the application of standard plasticity procedure.

This model is the first in attempting to address the irreversibility of ASR expansion through concepts of plasticity. As will be shown in the proceeding review, the evolution of plastic deformation here is caused applied stress only. For instance, the model does not allow permanent deformation for stress-free ASR expansion. It does however hint at the concept

of chemoplasticity that will be introduced in Chapter 3. Therefore, the deficiencies of this model will serve as motivation for the development of the new chemoplastic model.

Including the effects of temperature and ASR expansion, the total elastic strain is defined as follows:

$$\varepsilon = \mathbf{\Lambda}^e : \boldsymbol{\sigma} + \frac{1}{3}\varepsilon_A \mathbf{1} + \varepsilon_\theta \tag{2.62}$$

where $\mathbf{\Lambda}^e$ is the fourth order elastic compliance tensor, the scalar ε_A gives volumetric strain due to the expansion of the alkali-silica gel, and ε_θ is the thermal strain. The thermal expansion term simply accounts for expansion (or shrinkage) experienced by concrete due to temperature change and is defined as:

$$\varepsilon_\theta = \frac{1}{3}\alpha(\theta - \theta_0)\mathbf{1} \tag{2.63}$$

where α is the coefficient of thermal expansion for the concrete, and $(\theta - \theta_0)$ represents the change in temperature incurred for the period of measurement. Assuming the additivity of elastic and plastic strain increments, equation (2.62) is written in an incremental form for the elastoplastic regime:

$$d\varepsilon = \mathbf{\Lambda}^e : d\boldsymbol{\sigma} + d\mathbf{\Lambda}^e : \boldsymbol{\sigma} + \frac{1}{3}d\varepsilon_A \mathbf{1} + \frac{1}{3}\alpha d\theta \mathbf{1} + d\varepsilon^p \tag{2.64}$$

which can be rearranged as follows:

$$d\boldsymbol{\sigma} = \mathbf{C}^e[d\varepsilon - d\mathbf{\Lambda}^e : \boldsymbol{\sigma} - \frac{1}{3}d\varepsilon_A \mathbf{1} + \frac{1}{3}\alpha d\theta \mathbf{1} - d\varepsilon^p] \tag{2.65}$$

where $\mathbf{C}^e = (\mathbf{\Lambda}^e)^{-1}$. The terms including the elastic compliance imply that this material property is not constant. Indeed, the compliance is expected to degrade as a consequence of ASR expansion resulting in an overall loss of stiffness. The exact form employed to simulate this degradation of stiffness, as well as of strength, will be detailed later.

The evolution of the chemical reaction is described by the swelling rate, $\dot{\varepsilon}_A = \frac{d\varepsilon}{dt}$, and the development of this term requires the introduction of a number of new functions that consider time-temperature effects of ASR expansion and local constraints to this expansion. This scalar rate term is defined as follows:

$$\dot{\varepsilon}_A = \dot{g}_1(t')g_2(\sigma_m) \tag{2.66}$$

where $g_1 = g_1(t')$ quantifies ASR expansion free of external constraint, $g_2 = g_2(\sigma_m)$ is related to the constraint of hydrostatic pressure induced by the confining concrete with $\sigma_m = \frac{1}{3}tr(\boldsymbol{\sigma})$ the mean stress, and t' is a thermal activation time or "equivalent time", similar to the maturity concept employed in cement chemistry, and is given in the form:

$$dt' = g_3(\theta)dt \tag{2.67}$$

where $g_3 = g_3(\theta)$ represents constraints on expansion imposed by temperature θ, and t is real time. The functions, g_1, g_2, and g_3, were empirically chosen from experimental test data found in the literature. These three functions are formulated as follows:

$$g_1(t') = \frac{\epsilon t'}{A_1 + t'} \tag{2.68}$$

$$g_2(\sigma_m) = exp\left(\frac{3A_2\sigma_m}{f_{c0}}\right) \tag{2.69}$$

$$g_3(\theta) = \frac{1}{2}\left(1 + tanh\left(\frac{\theta - \theta_0}{A_3}\right)\right) \tag{2.70}$$

where A_1, A_2, and A_3 are material constants, and θ_0 is a reference temperature for which time t coincides with activation time t'; ϵ is the maximum strain for stress-free ASR expansion, and f_{c0} is the initial compressive strength of concrete. A closer examination of these functions reveals several interesting characteristics.

The function, $g_1(t')$, asymptotically approaches the maximum expansive strain, ϵ, as time progresses. Thus, this function gives directly the value for free gel expansion for a given time and temperature. Furthermore, $g_1(t')$ can be normalized, yielding a reaction extent term that varies between zero and one. To illustrate:

$$\xi = \frac{g_1}{\epsilon} \in [0, 1] \tag{2.71}$$

where $\xi = 0$ represents the beginning of the reaction, and $\xi = 1$ signifies the completion of the reaction. Now, the evolution of the reaction is derived as follows:

$$\dot{\xi} = \frac{1}{\epsilon}\frac{\partial g_1}{\partial t'}\frac{\partial t'}{\partial t} = \frac{(1-\xi)^2}{\tau} \tag{2.72}$$

which appears as the kinetics law of ASR in this model [to be compared with (2.61)]. Here a latency time is defined as $\tau = A_1/g_3(\theta)$. Furthermore, it also holds that $0 \leq g_2(\sigma_m) \leq 1$. The smaller the value of $g_2(\sigma_m)$, the greater the confining hydrostatic pressure at the site of expansion. A value of unity for $g_2(\sigma_m)$ would mean that the concrete skeleton offers no restraint to expansion, and consequently $\dot{g}_1(t')$, the free expansion term, would provide the only contribution to $\dot{\varepsilon}_A$ in equation (2.66). Lastly, the function, $g_3(\theta)$ is defined hyperbolically as varying between zero and one. This function controls the thermal activation time, such that very low temperatures cause the reaction to essentially stop ($dt' \rightarrow 0$), and at high temperatures the reaction proceeds in real time ($dt' \rightarrow dt$).

Finally, integration of this expression with $\xi = 0$ at $t = 0$ yields:

$$\xi = \frac{t}{\tau + t} \tag{2.73}$$

Equation (2.73) gives the reaction extent for any time t. With $\tau = 83$ days (as observed in experimental data for stress-free expansion [30]), a plot can be constructed showing the

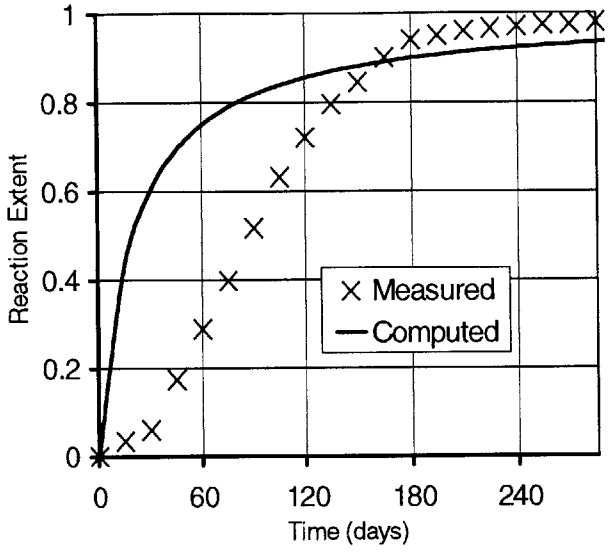

Figure 2.8: Predicted and measured reaction kinetics

extent of the stress-free reaction over time. The resulting curve can then be compared to actual test data to elucidate the effectiveness of the model at predicting reaction kinetics (Fig. 2.8). From this plot it can be seen that the model does not account for the initiation period at the beginning of the reaction, as the development period is shown to begin almost immediately. Additionally, the asymptotic expansion is approached in the model much more slowly than in the experimental data. A more accurate prediction of kinetics was shown in the previous model and will be incorporated into the chemoplasticity model of the next chapter.

The reaction kinetics having been established, the degradation of the concrete's mechanical properties can next be derived. The degradation of material properties depends on the

materials themselves and the extent of the ASR reaction:

$$E = E_0 \mu_1 \tag{2.74}$$

$$f_c = f_{c0} \mu_2 \tag{2.75}$$

where E and f_c are the current Young's modulus and compressive strength, respectively, the "0" subscript indicate original pre-reaction values, and $\mu_i = [1 - (1 - B_i)\xi]$. The material constants, B_i depend on both the material and the mechanical properties in question. Clearly, as $\xi \rightarrow 0$, $E \rightarrow B_1 E_0$ and $f_c \rightarrow B_2 f_{c0}$.

The condition for the onset of plastic deformation is defined by the yield surface, $f(\boldsymbol{\sigma}) = 0$:

$$f = \sqrt{J_2} - \beta(\gamma)\bar{\sigma}_c = 0 \tag{2.76}$$

in which J_2 is the second invariant of deviatoric stress, $\beta(\gamma)$ is a function that accounts for damage to the concrete matrix, and $\bar{\sigma}$ is the maximum value for $\sqrt{J_2}$ in compression. The evolution of plastic deformation $d\boldsymbol{\varepsilon}^p$ is determined by application of a non-associated plastic flow rule:

$$d\boldsymbol{\varepsilon}^p = d\lambda \frac{\partial g}{\partial \boldsymbol{\sigma}} \tag{2.77}$$

where $d\lambda$ is the plastic multiplier, specifying the intensity of plastic deformation, and $g(\boldsymbol{\sigma})$ is the plastic potential function:

$$g = \sqrt{J_2} - \eta_c \bar{I} \ln\left(\frac{\bar{I}}{\bar{I}_0}\right) = 0 \tag{2.78}$$

where η_c is a constant describing the point at which dilatation begins. Also, $\bar{I} = a_0 f_c + I_1$ and $\bar{I}_0 = e a_0 f_c$., where I_1 is the first invariant of the stress tensor, f_c is the compressive strength of concrete, while e and a_0 are material constants.

It should be noted here that based on the yield surface given in (2.76), plastic deformation is not possible in the stress-free case of ASR expansion. When $\boldsymbol{\sigma} = 0$, clearly $\sqrt{J_2} = \sqrt{\frac{1}{2}tr(\mathbf{s} \cdot \mathbf{s})}$ $= 0$, and the material parameters as defined in the literature, β and $\bar{\sigma}_c$, are always greater than zero. Thus, plasticity never occurs for this stress state, since $f < 0$. Intuitively, plastic strains do result from ASR swelling, even in the absence of an externally supplied stress. This point serves as further motivation for the new chemoplasticity model to be developed in the next chapter.

Chapter 3

ASR Chemoplasticity

The chemoplastic model of ASR expansion aims to predict macroscopic expansion by providing a link between the kinetics of the reaction and the irreversible structural deformation caused by the expansion. Furthermore, the model seeks to quantify the phenomenon of stress-induced anisotropy, as observed in test data. This chapter presents ASR chemoplasticity by first formulating the problem in terms of a 1-D rheological scheme that can be easily analyzed. A consideration of energy within the system then enables a straightforward extension to three dimensions. The framework of the model is completed with the introduction of a Drucker-Prager plasticity criterion. With the expansion equations now developed, the chemoplastic model is then completed with: (1) an identification of intrinsic material parameters, (2) a calibration of expansion equations to test data, and (3) a verification of the calibration procedure through a comparison of predicted and measured kinetics.

3.1 A 1-D Think Model for Chemomechanical Couplings

Swelling of chemical origin results from the relative volume increase between the product and reactant phases involved in the chemical reaction. The products expand in pores and microcracks of the cementitious matrix. Once this free expansion space is filled, the swelling is restrained, and the product phases exert locally a pressure on the surrounding concrete skeleton. This mesoscopic mechanism is roughly sketched in Figure 2.5. For stress-free concrete the internal swelling pressure p_s of the expansive products is self balanced by tension σ_μ in the skeleton. Consequently, the overall material swells.

3.1.1 1-D Chemoelastoplasticity

The first model to be examined here involves the case of chemoelastoplasticity [34]. This model captures expansive material behavior at a macrolevel of material description, i.e. at the typical scale of laboratory test specimens. The simplest rheological device that can describe an irreversible skeleton deformation coupled with the swelling pressure is shown in Figure 3.1, in the form of an elastoplastic spring device in parallel with a chemical pressure cell. In this figure, σ is the macroscopic stress due to external forces, and ϵ the corresponding overall strain. σ_μ denotes the stress in the spring of stiffness E_m, and p_s is the swelling pressure in the chemical pressure cell. ξ is the extent of this chemical reaction, and it is assumed that the volume increase of the products is proportional to the reaction extent, i.e. $\phi_s = \kappa\xi$. With ϵ^p as the displacement of the friction device of strength k_m associated with the permanent

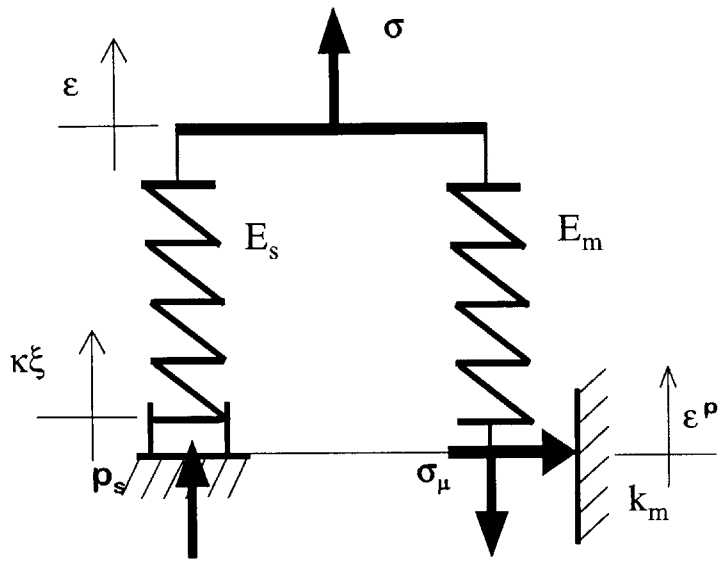

Figure 3.1: Rheological representation of ASR chemoelastoplasticity

strain in the matrix, the stress in this 1-D chemoelastoplastic model reads:

$$\sigma = \sigma_\mu - p_s = (E_m + E_s)\varepsilon - E_m\varepsilon^p - E_s\kappa\xi \tag{3.1}$$

with:

$$\sigma_\mu = E_m(\varepsilon - \varepsilon^p); \quad -p_s = E_s(\varepsilon - \kappa\xi) \tag{3.2}$$

In addition, the stress exerted on the friction device is the stress $\sigma_\mu = \sigma + p_s$, and the plasticity criterion can be written in the form:

$$f(\sigma, p_s) = |\sigma + p_s| - k_m \leq 0 \tag{3.3}$$

To illustrate the effect of the swelling pressure p_s on irreversible and total deformation of

the reference system, a stress-free expansion test is considered. From (3.1) and (3.2), the following formulation is obtained:

$$\sigma = 0; \quad p_s = E_s\left[(\kappa - \beta)\xi - \phi_s^p\right]; \quad \varepsilon = \beta\xi + \phi_s^p \tag{3.4}$$

where $E = E_m + E_s$, and $\beta = \kappa E_s/E < \kappa$. Furthermore, $\phi_s^p = \frac{E_m}{E}\epsilon^p$ denotes the expansion space which is irreversibly formed when the swelling pressure reaches the material strength of the matrix k_m. Now, the following can be concluded:

- For $\xi < \xi_0 = k_m/[E_s(\kappa - \beta)]$, the system behaves chemoelastically $(\dot{\epsilon}^p = \dot{\phi}_s^p = 0)$:

$$\xi < \xi_0 : d\varepsilon = \beta d\xi \tag{3.5}$$

  In this chemoelastic phase, the total strain increment $d\epsilon$ is related through a chemical dilatation coefficient $\beta = \kappa E_s/E$ to the reaction extent $d\xi$ of the chemical reaction. This chemical dilatation coefficient depends on the intrinsic dilatation coefficient κ of the reaction products, and on the stiffness of the overall material $E = E_m + E_s$ [24]. Due to the elastic stiffness of the matter restraining the free expansion of the reaction products in the deformable medium, β is smaller than the intrinsic chemical dilatation coefficient of the reaction products κ.

- For $\xi = \xi_0 = k_m/[E_s(\kappa - \beta)]$, the swelling pressure reaches the material strength, $f = 0 \leftrightarrow |p_s| = k_m$, which it cannot exceed for $\xi > \xi_0$ in the considered case of a perfect plastic behavior of the matrix. In order for the swelling pressure to remain constant, irreversible skeleton deformation must occur, providing pressure free expansion space for the newly formed products. This concept can be expressed by the 1-D chemoplastic consistency

condition:

$$\xi > \xi_0 : df = dp_s \operatorname{sign}(p_s) = 0 \leftrightarrow d\phi_s^p = (\kappa - \beta) d\xi \tag{3.6}$$

This chemoplastic deformation amplifies the chemoelastic response (3.5) according to:

$$\xi > \xi_0 : d\varepsilon = \kappa d\xi \tag{3.7}$$

which after integration becomes:

$$\varepsilon = \beta\xi + (\kappa - \beta)\langle \xi - \xi_0 \rangle \tag{3.8}$$

where $\langle x \rangle = \frac{1}{2}(x + |x|)$. The first term represents the purely elastic volume increase caused by the expansion products in the deformable medium. In turn, the second term represents the irreversible volume increase ϕ_s^p associated with a permanent deformation of the matrix.

As in the chemoelastic case, the evolution of ξ is defined by a kinetics law of the form (2.45), which is here recalled:

$$1 - \xi = t_c \frac{d\xi}{dt} \tag{3.9}$$

where t_c is a characteristic time of the reaction, to be determined experimentally. Larive's formula (2.48) was determined from the relative stress-free expansion $\xi \equiv \bar{\xi} = \varepsilon(t)/\varepsilon(\infty)$, here recalled:

$$t_c = \tau_c(\theta) \frac{1 + \exp[-\tau_L(\theta)/\tau_c(\theta)]}{\bar{\xi} + \exp[-\tau_L(\theta)/\tau_c(\theta)]} \tag{3.10}$$

with τ_L and τ_c,the latency time and the characteristic time, respectively, sketched in Figure 3.2. These time constants follow the Arrhenius concept as shown in Figure 3.3 [24, 34].

$$\tau_L(\theta) = \tau_L(\theta_0) \exp[U_L(1/\theta - 1/\theta_0] \tag{3.11}$$

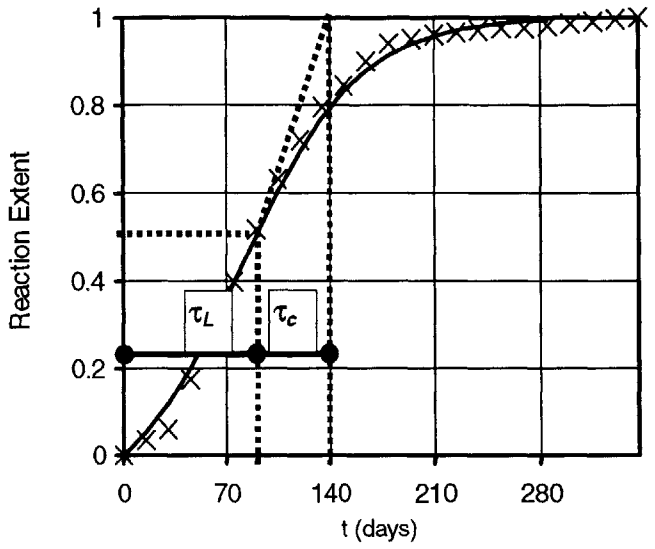

Figure 3.2: Stress-free ASR expansion curve showing τ_L and τ_c [34]

$$\tau_c(\theta) = \tau_c(\theta_0) \exp[U_c(1/\theta - 1/\theta_0] \tag{3.12}$$

where $\tau_L(\theta_0)$ and $\tau_c(\theta_0)$ are the time constants at reference temperature θ_0, and $U_L = 9,400 \pm 500$ K and $U_c = 5,400 \pm 500$ K are thermal activation constants. A comparison of these thermal activation constants of macroscopic ASR expansion to the activation constants of microscopic in vitro silica dissolution and in vitro ASR gel formation reveals the nature of the two time constants. As such, τ_L and τ_c are found to be associated with the dissolution of reactive silica and with the mechanism of gel formation, respectively. At constant temperature, $\theta = \theta_0$, Larive's kinetics law (3.9) with (3.10) integrates to the characteristic $s-$curve of ASR-expansion (2.47), which is recalled:

$$\bar{\xi}(t) = \frac{\varepsilon(t)}{\varepsilon(\infty)} = \frac{1 - \exp(-t/\tau_c)}{1 + \exp(-t/\tau_c + \tau_L/\tau_c)} \tag{3.13}$$

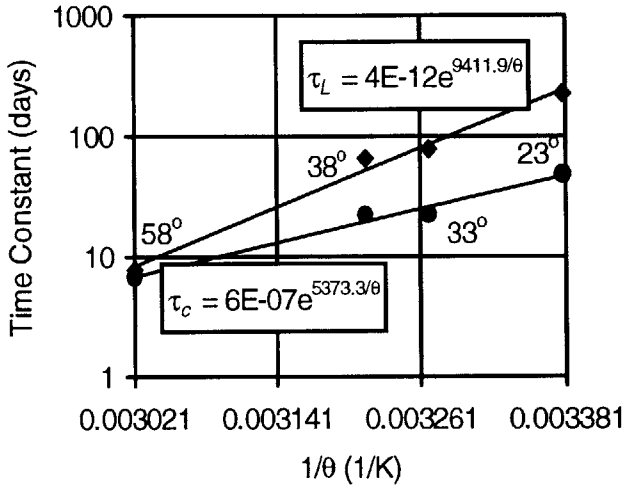

Figure 3.3: Arrhenius plot of τ_L and τ_c [24, 34]

This function together with the experimental values is shown in Figure 3.2. Finally, it is instructive to study the limit cases of (3.8): For $\xi_0 \to 1$, the chemomechanical response is governed by chemoelastic evolution, i.e. $\varepsilon = \beta\xi$ and $\phi_s^p \to 0$. This approach has been used to determine the macroscopic reaction kinetics (3.10) and is based on the assumption of a pure elastic skeleton behavior. For the case in which $0 \leq \xi_0 < 1$, and $\kappa \gg \beta \leftrightarrow E_s/E \ll 1$, free expansion space is primarily generated by the irreversible skeleton deformations associated with microcracking and fracture in the matrix, i.e. in a stress free experiment $\phi_s^p = \frac{E_m}{E}\varepsilon^p \approx \varepsilon^p$ and $E \approx E_m$. The rheological scheme associated with these two limit cases are sketched in Figures 3.4 and 3.5. The first case (Fig. 3.4) of a pure chemoelastic coupling was considered in the previous chapter[24, 30, 34], while the second case (Fig. 3.5) is the focus of this chapter.

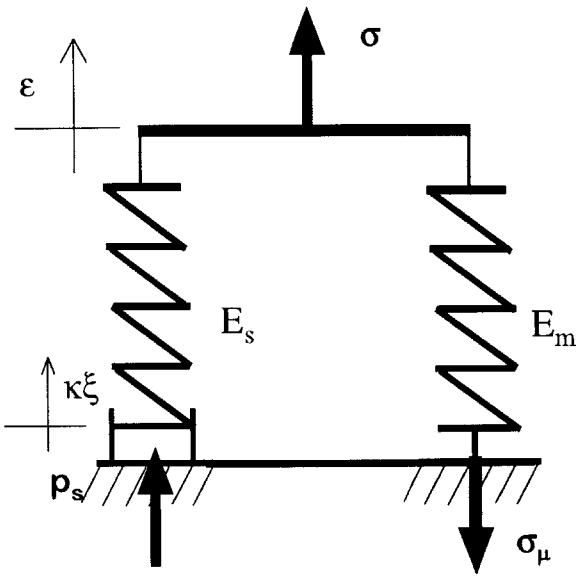

Figure 3.4: Rheological representation of chemoelasticity [34]

3.1.2 1-D Chemoplastic Expansion

The rheological device (Fig. 3.5) corresponding to the second limit case of chemoelastoplasticity forms the basis for the chemoplasticity model. By means of this device, the energy transformation that occurs during chemoplastic evolutions is examined. As was the case for the chemoelasticity model of the previous chapter, the starting point here is the Clausius-Duhem inequality, which for the 1-D reference system reads:

$$\varphi dt = \sigma d\varepsilon - d\psi \geq 0 \tag{3.14}$$

where $\sigma d\varepsilon$ is the strain energy and ψ is the Helmholtz (free) energy. For the chemoplastic think model, the Helmholtz energy can be written in the form:

$$\psi = \frac{1}{2}\left[E(\varepsilon - \varepsilon^p)^2 + E_s(\phi_s^p - \kappa\xi)^2\right] + g(\xi) \tag{3.15}$$

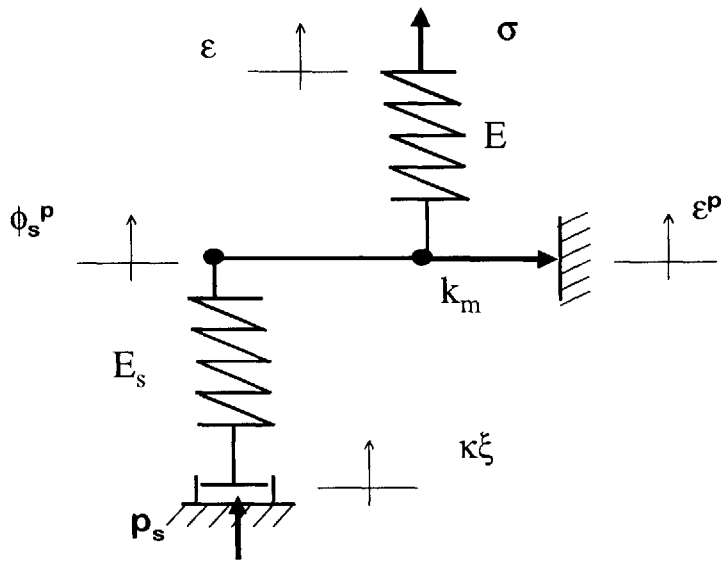

Figure 3.5: Rheological representation of ASR chemoplasticity

The first term in the bracket of (3.15) represents the free energy of the overall elasticity and the second term the elastic energy of the hardening spring of modulus E_s. Finally, function $g(\xi)$ corresponds to the free energy in the chemical pressure cell. Use of (3.15) in (3.14) yields:

$$\varphi dt = \sigma d\varepsilon^p + p_s d\phi_s^p + A_m d\xi \geq 0 \tag{3.16}$$

together with:

$$\sigma = \frac{\partial \psi}{\partial \varepsilon} = -\frac{\partial \psi}{\partial \varepsilon^p} = E(\varepsilon - \varepsilon^p) \tag{3.17}$$

$$p_s = -\frac{\partial \psi}{\partial \phi_s^p} = E_s \left[\kappa\xi - \phi_s^p\right] \tag{3.18}$$

$$A_m = -\frac{\partial \psi}{\partial \xi} = -\kappa p_s - \frac{\partial g}{\partial \xi} \tag{3.19}$$

The first term in (3.16) is the standard term of elastoplasticity, which identifies the stress σ as the driving force of the permanent deformation increment $d\varepsilon^p$. In the same way, the second

term in (3.16) identifies the swelling pressure p_s as driving force associated with the plastic expansion space $d\phi_s^p$. This formal identification implies that the complementary evolution laws of plastic strain and permanent expansion both relate the driving force to the rate. In the framework of chemoplasticity, these complementary evolution laws read [40]:

$$d\varepsilon^p = d\lambda \frac{\partial f}{\partial \sigma} = d\lambda \text{sign}(\sigma + p_s) \quad d\phi_s^p = d\lambda \frac{\partial f}{\partial p_s} = d\lambda \text{sign}(\sigma + p_s) \tag{3.20}$$

where $d\lambda$ is the plastic multiplier and $f(\sigma, p_s) \leq 0$ the chemoplastic loading function (3.3). A loading point defined by stress σ and swelling pressure p_s that is situated at the loading surface (i.e. $f(\sigma, p_s) = 0$) remains on it (i.e. $df = 0$). This is expressed by the consistency condition,

$$df = \frac{\partial f}{\partial \sigma} d\sigma + \frac{\partial f}{\partial p_s} dp_s = 0 \tag{3.21}$$

Use of the state equation (3.18) and of the plastic expansion rule $(3.20)_2$ in (3.21), delivers the plastic multiplier in the form:

$$d\lambda = \frac{1}{H} \left[\frac{\partial f}{\partial \sigma} d\sigma + \frac{\partial f}{\partial p_s} E_s \kappa d\xi \right] = \left[\frac{d\sigma}{H} + \frac{E_s}{H} \kappa d\xi \right] \text{sign}(\sigma + p_s) \tag{3.22}$$

where H appears as a hardening modulus, defined by:

$$H = E_s \left(\frac{\partial f}{\partial p_s} \right)^2 = E_s \tag{3.23}$$

Hence, the swelling pressure in this chemoplastic model plays the role of a hardening force, which depends on both the hardening variable ϕ_s^p and on the reaction extent ξ. This type of chemoplastic model has originally been proposed in Coussy and Ulm (1996) [40].

Finally, the last term of the formulation in (3.16) represents that part of the dissipation associated with the chemical reaction, and affinity A_m (3.19) is the driving force associated

in this dissipation (3.16) with the increase in reaction extent $d\xi$:

$$A_m d\xi = -\left[\kappa p_s + \frac{\partial g}{\partial \xi}\right] d\xi \geq 0 \tag{3.24}$$

The first term $-p_s \kappa d\xi$ represents the expansion work of the newly formed products in the porous medium. In a stress-free experiment, according to (3.20) and (3.22), this work is consumed by the plastic dissipation $p_s d\phi_s^p = p_s \kappa d\xi = k_m d\varepsilon^p$, and the effective transformation of useful mechanical work into heat form during time interval dt reads:

$$\sigma = 0, p_s = k_m : \varphi dt = -\frac{\partial g}{\partial \xi} d\xi \geq 0 \tag{3.25}$$

With (3.25), $\mathcal{A}(\xi) = -\partial g / \partial \xi$ is formally identified as the driving force of the chemical reaction in a stress-free experiment and has been implicitly used when writing the chemical kinetics law (3.9). This identification still holds when a constant stress σ_0 is applied during ASR-expansion (i.e. $d\sigma = 0 \hookrightarrow \varphi dt = \sigma_0 d\varepsilon^p + \mathcal{A}(\xi) d\xi \geq 0$) and can be generalized to an arbitrary stress history $\sigma = \sigma(t)$, provided that the macroscopic chemical affinity A_m depends significantly only on reaction extent ξ. In this case, the linear kinetics law (3.9) still applies under macroscopic stress application:

$$\forall \sigma : A_m \simeq \mathcal{A}(\xi) = -\frac{\partial g}{\partial \xi} \equiv \mathcal{A}_0 (1 - \xi) = k_d \frac{d\xi}{dt} \hookrightarrow t_c \frac{d\xi}{dt} = 1 - \xi \tag{3.26}$$

where $t_c = k_d / \mathcal{A}_0$ of the form (3.10) is the characteristic time of the chemical reaction. Once t_c is known, the 1-D chemoplastic model is complete.

3.2 3-D Chemoplasticity of ASR Expansion

3.2.1 Formulation

The extension of the chemoplasticity model to the 3-D case involves replacing the scalar quantities of the 1-D model by their tensorial counterparts. Hence, the dissipation (3.16) reads:

$$\varphi dt = \boldsymbol{\sigma} : d\boldsymbol{\varepsilon^p} + p_s d\phi_s^p + A_m d\xi \geq 0 \tag{3.27}$$

The state equations (3.17), (3.18), and (3.19) become in the isotropic case:

$$\boldsymbol{\sigma} = \frac{\partial \psi}{\partial \boldsymbol{\varepsilon}} = -\frac{\partial \psi}{\partial \boldsymbol{\varepsilon^p}} = \left(K - \frac{2}{3}G\right)(\epsilon - \epsilon^p)\mathbf{1} + 2G\left(\boldsymbol{\varepsilon} - \boldsymbol{\varepsilon^p}\right) \tag{3.28}$$

$$p_s = -\frac{\partial \psi}{\partial \phi_s^p} = K_s\left[3\kappa\xi - \phi_s^p\right] \tag{3.29}$$

$$A_m = -\left[\kappa p_s + \frac{\partial g}{d\xi}\right] \simeq -\frac{\partial g}{d\xi} = \mathcal{A}_0(1-\xi) \tag{3.30}$$

where $\epsilon = tr(\boldsymbol{\varepsilon})$, $\epsilon^p = tr(\boldsymbol{\varepsilon^p})$, while K and G are the overall bulk and shear modulus, respectively. From standard plasticity theory, a loading function f defines the elasticity domain D_E:

$$(\boldsymbol{\sigma}, p_s) \in D_E \leftrightarrow f(\boldsymbol{\sigma}, p_s) \leq 0 \tag{3.31}$$

The complementary evolution laws are the plastic flow rules:

$$d\boldsymbol{\varepsilon^p} = d\lambda \frac{\partial h}{\partial \boldsymbol{\sigma}}; \qquad d\phi_s^p = d\lambda \frac{\partial h}{\partial p_s} \tag{3.32}$$

and the kinetics law (3.26). In (3.32), h is the plastic potential, and $d\lambda$ is the plastic multiplier:

$$d\lambda = \frac{1}{H}\left[\frac{\partial f}{\partial \boldsymbol{\sigma}} d\boldsymbol{\sigma} + \frac{\partial f}{\partial p_s} 3K_s\kappa d\xi\right] \tag{3.33}$$

and H the hardening modulus,

$$H = K_s' \left(\frac{\partial f}{\partial p_s}\right)\left(\frac{\partial h}{\partial p_s}\right) \tag{3.34}$$

where $K_s' = -\partial p_s / \partial \phi_s^p$. In the case of a linear plastic hardening behavior $K_s' = K_s$. In turn, a non-linear plastic hardening corresponds to $K_s = K_s(\phi_s^p)$ and $K_s' = K_s - p_s/K_s(\partial K_s/\partial \phi_s^p)$.

Once the loading function f and the plastic potential h are specified, the 3-D model is complete.

3.2.2 Stress-Induced Anisotropy of Chemical Expansion

To illustrate chemoplasticity, a simple, hydrostatic pressure-dependent yield criterion, the Drucker-Prager loading surface is considered in the form:

$$f(\boldsymbol{\sigma}, p_s) = \sqrt{J_2} + \alpha(\sigma_m + p_s) - c \leq 0 \tag{3.35}$$

where J_2 and σ_m are the invariants $J_2 = \frac{1}{2}tr(\mathbf{s}\cdot\mathbf{s})$ and $\sigma_m = \frac{1}{3}tr(\boldsymbol{\sigma})$, respectively; $\mathbf{s}$ is the stress deviator, α is the friction coefficient of the concrete, and c is the cohesion.

The requisite condition for plastic deformation having been established by (3.35), the evolution of this deformation can then be described by the plastic flow rules. Assuming an associated plastic potential ($f = h$) the flow rules (3.32) read:

$$d\boldsymbol{\varepsilon}^p = d\lambda\left[\frac{\mathbf{s}}{2\sqrt{J_2}} + \frac{1}{3}\alpha\mathbf{1}\right] \qquad d\phi_s^p = d\lambda\frac{\partial f}{\partial p_s} = d\lambda\alpha = d\epsilon^p \tag{3.36}$$

where $\epsilon^p = tr(\boldsymbol{\varepsilon}^{\boldsymbol{p}})$ is the volumetric strain, and the plastic multiplier is:

$$d\lambda = \frac{1}{H}\left[d\sqrt{J_2} + \alpha(d\sigma_m + 3K_s\kappa d\xi)\right] \tag{3.37}$$

where $H = \alpha^2 K_s'$. In the equation $(3.36)_1$, the first term in the brackets physically represents the deviatoric portion of expansion, while the second term accounts for pure volumetric expansion. With all the necessary relations in hand, the incremental strain tensor $(3.36)_1$ can be now studied for different loading cases. Because cylindrical test samples were used in testing, only two directions need to be examined due to symmetry about their longitudinal axes.

Under stress-free conditions, for $\xi_0 = c/3\kappa K_s \alpha \leftrightarrow f = 0$, the following relations are obtained from (3.28), (3.36) and (3.37):

$$d\boldsymbol{\varepsilon} = d\boldsymbol{\varepsilon}^{\boldsymbol{p}} = \bar{\kappa} d\xi \mathbf{1} \quad d\phi_s^p = 3\bar{\kappa} d\xi = d\epsilon^p \tag{3.38}$$

where $\bar{\kappa} = \kappa K_s / K_s'$.

Next a uniaxial stress state ($\sigma_{11} = \sigma$) is considered. This stress is applied at $t = 0$ and held constant in time. The deviatoric stress tensor, s, defined as the difference between the overall stress tensor and hydrostatic stress tensor, $\sigma_m \mathbf{1}$, takes the following form under uniaxial stress:

$$(s_{ij}) = \frac{1}{3} \begin{pmatrix} 2\sigma & 0 & 0 \\ 0 & -\sigma & 0 \\ 0 & 0 & -\sigma \end{pmatrix} \tag{3.39}$$

It follows directly that the second invariant of the stress deviator is:

$$J_2 = \frac{1}{2} tr(\mathbf{s} \cdot \mathbf{s}) = \frac{\sigma^2}{3} \tag{3.40}$$

For $t > 0$ and with $d\lambda = 3\bar{\kappa} d\xi / \alpha$, independent of stress application, the plastic volume expansion still reads:

$$d\phi_s^p = 3\bar{\kappa} d\xi = d\epsilon^p \tag{3.41}$$

The strain increments in the direction of stress application read:

$$d\varepsilon_{11} = d\varepsilon_{11}^{p} = \bar{\kappa} d\xi \left[\frac{\sqrt{3}}{\alpha} \mathrm{sign}(\sigma) + 1 \right] \tag{3.42}$$

and normal to direction 1:

$$d\varepsilon_{22} = d\varepsilon_{22}^{p} = \bar{\kappa} d\xi \left[-\frac{\sqrt{3}}{2\alpha} \mathrm{sign}(\sigma) + 1 \right] \tag{3.43}$$

and $d\varepsilon_{33} = d\varepsilon_{33}^{p} = d\varepsilon_{22}$. The previous equations show the stress induced anisotropy of expansive reactions which provokes irreversible skeleton deformation at a mesoscopic level. In the macroscopic chemoplastic model, this results from the dependency of the plastic strain on the deviator stress. Hence, letting $\gamma = d\varepsilon_{11}/d\varepsilon_{22}$ the slope of two strain components measured in a stressed ASR-expansion test, the friction coefficient α can be determined:

$$\alpha = -\sqrt{3} \frac{1 + \gamma/2}{1 - \gamma} \mathrm{sign}(\sigma) \tag{3.44}$$

At the same time, the relevance of the modeling can be checked through the determination of the friction coefficient α of a non-reactive control specimen, from the uniaxial compressive strength f_c' and the uniaxial tension strength f_t'. For $p_s = 0$, friction coefficient α and cohesion c can be assessed from (3.35) by:

$$\alpha = \sqrt{3} \frac{1 - f_t'/f_c'}{1 + f_t'/f_c'}; \quad \frac{c}{f_t'} = \frac{2}{\sqrt{3}(1 + f_t'/f_c')} \tag{3.45}$$

Hence, provided similar values of α determined from (3.44) and (3.45), not only will the consistency of the determination process be verified, but simultaneously the relevance of the proposed chemoplastic model: the expansive reaction in the concrete sample activates the same fracture processes as a macroscopic stress application which reaches the material strengths, f_t' and f_c'.

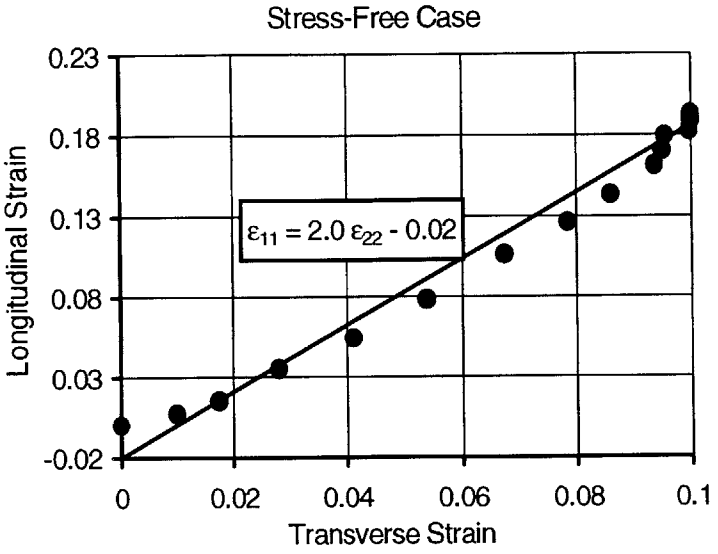

Figure 3.6: Anisotropic expansion of stress-free specimen

3.2.3 Larive's Stressed Expansion Tests

In a recent test campaign [30], Larive performed expansion tests on stress-free and compression-stressed cylinder samples. In all tests, the longitudinal strain ε_{11} and the radial strain ε_{22} were recorded as a function of time. It was checked that both follow the same kinetics. However, under stress-free conditions, a surprising anisotropic behavior was found (Fig. 3.6). The slope $\gamma_{\sigma=0} = d\varepsilon_{11}/d\varepsilon_{22}$ shown in Figure 3.6 is not unity, but approximately $\gamma_{\sigma=0} = 2$.

This anisotropy was explained by the molding process of the cylinder samples, with water being trapped in pockets below the aggregates in the direction of the cylinder axis, which corresponds to direction 1, the direction of load application.

To explore Larive's tests, this initial molding anisotropy must be accounted for by considering

for the stress-free experiment a relation of the form:

$$d\boldsymbol{\varepsilon}^{\boldsymbol{p}} = \mathbf{b} d\phi_s^p \tag{3.46}$$

which results in a non-associated plastic potential $h \neq f$ in (3.32) of the form:

$$h(\boldsymbol{\sigma}, p_s) = \sqrt{J_2} + \alpha(\mathbf{b} : \boldsymbol{\sigma} + p_s) - c \tag{3.47}$$

In fact, use of (3.47) in (3.32) gives:

$$d\boldsymbol{\varepsilon}^{\boldsymbol{p}} = d\lambda \left[\frac{\mathrm{s}}{2\sqrt{J_2}} + \alpha \mathbf{b} \right]; \;\; d\phi_s^p = d\lambda \frac{\partial f}{\partial p_s} = d\lambda \alpha \tag{3.48}$$

In the isotropic case, $\mathbf{b}=\frac{1}{3}\mathbf{1}$. For the molding anisotropy, we preserve the diagonal structure of $\mathbf{b}=diag[b_{11}, b_{22}, b_{33}]$, and $tr(\mathbf{b}) = 1$ ensures that $tr(d\boldsymbol{\varepsilon}^{\boldsymbol{p}}) = d\phi_s^p$. For the stress free expansion test, it can be seen that:

$$d\varepsilon_{11}^p = d\lambda \alpha b_{11}; \;\; d\varepsilon_{22}^p = d\lambda \alpha b_{22} = d\varepsilon_{33}^p = d\lambda \alpha b_{33} \tag{3.49}$$

Thus,

$$\gamma_{\sigma=0} = \frac{d\varepsilon_{11}}{d\varepsilon_{22}} = \frac{d\varepsilon_{11}^p}{d\varepsilon_{22}^p} = \frac{b_{11}}{b_{22}} \tag{3.50}$$

and with (3.46):

$$b_{11} = \frac{\gamma_{\sigma=0}}{\gamma_{\sigma=0} + 2}; \;\; b_{22} = b_{33} = \frac{1}{\gamma_{\sigma=0} + 2} \tag{3.51}$$

In Larive's stress-free expansion test on 34 samples, for which $\gamma_{\sigma=0} = 1.967 \pm 0.294$, we determine $b_{11} = 0.493 \pm 0.038$ and $b_{22} = 0.253 \mp 0.019$. Under uniaxial constant stress application, (3.48) gives:

$$d\varepsilon_{11} = d\varepsilon_{11}^p = \bar{\kappa} d\xi \left[\frac{\sqrt{3}}{\alpha} \mathrm{sign}(\sigma) + 3b_{11} \right] \tag{3.52}$$

$$d\varepsilon_{22} = d\varepsilon_{22}^p = \bar{\kappa} d\xi \left[-\frac{\sqrt{3}}{2\alpha} \mathrm{sign}(\sigma) + 3b_{22} \right] \tag{3.53}$$

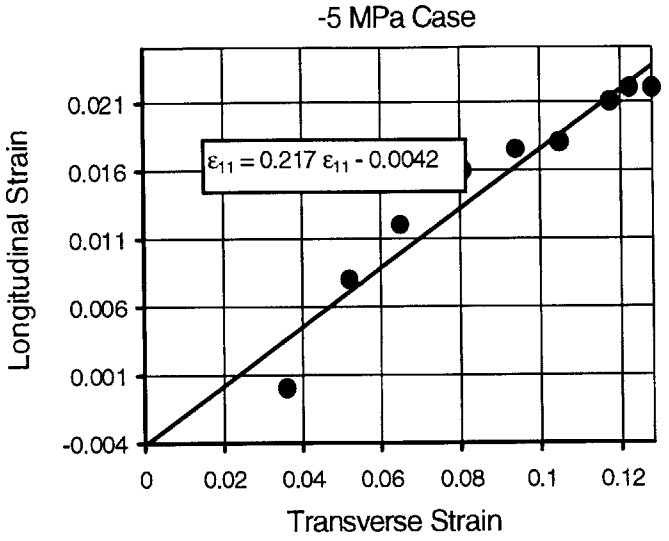

Figure 3.7: Determination of γ for 5 MPa compression case

and the slope $\gamma = d\varepsilon_{11}/d\varepsilon_{22}$ leads to:

$$\alpha = -\sqrt{3}\frac{1+\gamma/2}{3(b_{11}-\gamma b_{22})}\text{sign}(\sigma) \tag{3.54}$$

From Figures 3.7 and 3.8, the slopes γ of Larive's stressed expansion tests can be determined, and from (3.54) the friction coefficient α:

$$\boxed{\sigma = -5 \text{ MPa};\ \gamma_{\sigma=-5} = 0.217 \rightarrow \alpha = 1.47 \pm 0.15} \tag{3.55}$$

$$\boxed{\sigma = -10 \text{ MPa};\ \gamma_{\sigma=-10} = 0.182 \rightarrow \alpha = 1.42 \pm 0.14} \tag{3.56}$$

The results differ by about 4% indicating a fair amount of consistency of the determination process. However, what is most remarkable is that this friction coefficient $\alpha = 1.45$ is of the same magnitude as the one to be determined from the material strengths of the non-reactive samples (3.45). In Larive's series of tests, both the compressive strength and the

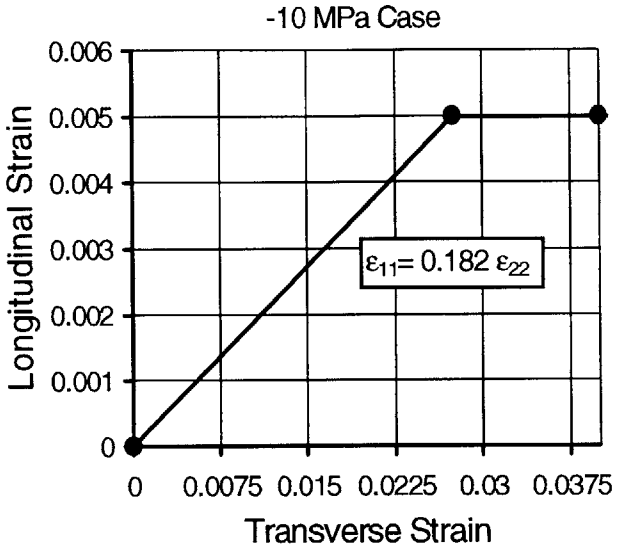

Figure 3.8: Determination of γ for 10 MPa compression case

(Brasilian) tension strength were monitored over the entire test duration on non-reactive control specimens kept under the same hygral and thermal conditions as the reactive test samples. The experimental results shown in Figure 3.9 indicate an almost constant tension strength to compression strength ratio of $f_t'/f_c' = 0.072$. Use of this value in (3.45) gives:

$$\boxed{p_s = 0; \frac{f_t'}{f_c'} = 0.068 \rightarrow \alpha = 1.50 \pm 0.03} \tag{3.57}$$

This value determined from pure mechanical strength tests (almost) coincides with the one determined from the stress induced expansion behavior (3.55) and (3.56), and proves that the frictional mechanisms activated by the swelling pressure are the same ones which are activated during concrete fracture, when the applied stress (in a non-reactive sample) reaches the material strength.

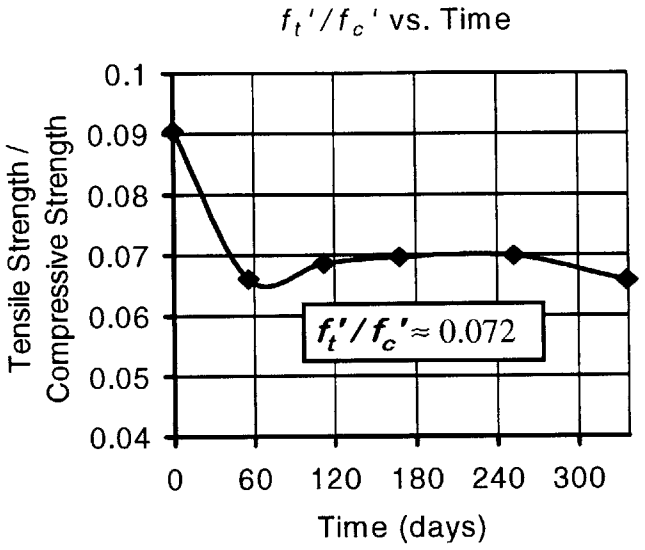

Figure 3.9: Tensile to compressive strength ratio

3.2.4 Model Calibration

The calibration process can now be completed through the determination of the intrinsic chemical expansion coefficient κ. This computation is somewhat more difficult to achieve, as it involves strain amplitudes rather than strain increments. Indeed, for a constant stress applied at $t = 0$, the volume expansion at $t > 0$ is given in the model by:

$$d\epsilon = d\epsilon^p = d\phi_s^p = 3\bar{\kappa} d\xi \tag{3.58}$$

and integrates to:

$$\epsilon(t) - \epsilon(0) = \epsilon^p(t) - \epsilon^p(0) = \phi_s^p(t) - \phi_{s0}^p = 3\bar{\kappa} \langle \xi(t) - \xi_0 \rangle \tag{3.59}$$

where $\epsilon(0)$ is the volume strain at load application (elastic and eventually plastic, i.e. $\epsilon^p(0)$), ξ_0 is the reaction extent at the onset of plastic deformation (i.e. $f = 0$), and ϕ_{s0}^p denotes the

Stress [MPa]	0	-5	-10	-20
$\delta\varepsilon_{11} \equiv \varepsilon_{11}(\infty) - \varepsilon_{11}(0)$ [%]	0.199	0.023	0.014	-0.003
$\delta\varepsilon_{22} \equiv \varepsilon_{22}(\infty) - \varepsilon_{22}(0)$ [%]	0.102	0.153	0.208	0.125
$\delta\epsilon \equiv \epsilon(\infty) - \epsilon_0$ [%]	0.403	0.329	0.430	0.247
$\bar{\kappa} = \kappa K_s/K_s'$ [%]	0.135	0.120	0.147	0.087
$\bar{p}_s$ [MPa]	3.1	6.2	9.3	15.5
$\kappa/\bar{\kappa} \equiv K_{s0}/K_s$	1.08	1.35	0.98	1.66
ϕ^p_{s0} [%]	1	2	1	5

Table 3.1: Experimental values and model parameters of Larive's ASR-expansion tests under compressive stress application.

initial plastic porosity in the material, which corresponds to the pressure free expansion space for the reaction products in the cementitious matrix (i.e. flaws, cracks, pores). In (3.59), it is implicitly assumed that $\bar{\kappa} = \kappa K_s/K_s'$ changes significantly only during load application, i.e. $K_s = K_s(\phi^p_{s0})$ and $K_s' = K_s[1 - (\partial K_s/\partial\phi^p_{s0})\bar{p}_s/K_s^2] = \textit{constant}$ during chemoplastic evolutions; thus

$$\kappa = \bar{\kappa}\left[1 - \frac{\partial K_s}{\partial \phi^p_{s0}}\frac{\bar{p}_s}{K_s^2}\right] \tag{3.60}$$

where $\bar{p}_s$ is the swelling pressure at the onset of plastic deformation, which, according to (3.35), remains constant throughout the chemoplastic deformation process under uniaxial stress application:

$$f = 0 \leftrightarrow p_s(\xi, \phi^p_s) = \bar{p}_s = \frac{c}{\alpha} - \frac{|\sigma|}{\alpha\sqrt{3}} - \sigma \tag{3.61}$$

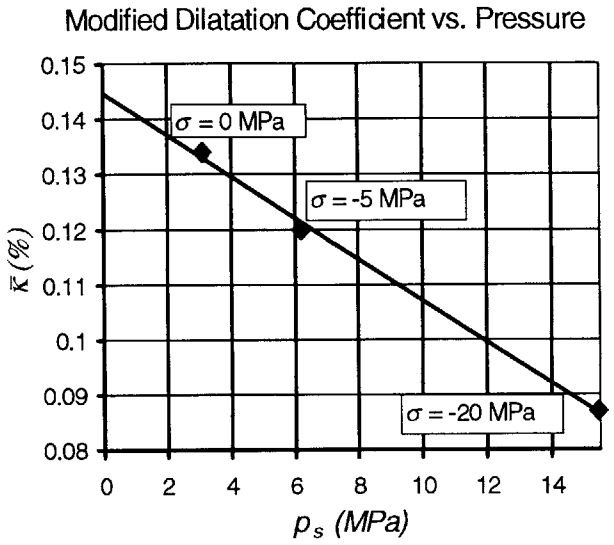

Figure 3.10: Variation of dilatation with increasing confinement pressure

The values of $\bar{p}_s$ determined with the help of (3.45) and (3.61) are given in Table 3.1. In addition, if it is assumed that $\xi_0 \ll 1$ in Larive's test, (3.59) can be rewritten in the form:

$$\xi_0 \ll 1 : \epsilon(t) - \epsilon(0) = 3\bar{\kappa}\xi(t) \tag{3.62}$$

With the same assumptions, (3.52) and (3.53) integrate to:

$$\varepsilon_{11}(t) - \varepsilon_{11}(0) = \varepsilon^p_{11}(t) - \varepsilon^p_{11}(0) = \bar{\kappa}\xi(t)\left[\frac{\sqrt{3}}{\alpha}\text{sign}(\sigma) + 3b_{11}\right] \tag{3.63}$$

$$\varepsilon_{22}(t) - \varepsilon_{22}(0) = \varepsilon^p_{22}(t) - \varepsilon^p_{22}(0) = \bar{\kappa}\xi(t)\left[-\frac{\sqrt{3}}{2\alpha}\text{sign}(\sigma) + 3b_{22}\right] \tag{3.64}$$

In Larive's tests, strain measurements started after 14 days of curing (3 days storage in an environmental chamber at 23°C and 98% RH, followed by 11 days of sealed storage at 23°C). The samples were then put in a humidity chamber at 38°C, the load was applied and kept constant in time. Additionally, strain measurements were carried out on non-reactive samples

	$\sigma = 0$		$\sigma = -5$ MPa	
	Test [%]	Model [%]	Test [%]	Model [%]
$\varepsilon_{11}(\infty) - \varepsilon_{11}(0)$	0.199	0.198	0.023	0.035
$\varepsilon_{22}(\infty) - \varepsilon_{22}(0)$	0.102	0.102	0.153	0.143
$\epsilon(\infty) - \epsilon(0)$	0.403	0.402	0.329	0.321
	$\sigma = -10$ MPa		$\sigma = -20$ MPa	
	Test [%]	Model [%]	Test [%]	Model [%]
$\varepsilon_{11}(\infty) - \varepsilon_{11}(0)$	0.014	0.048	-0.003	0.028
$\varepsilon_{22}(\infty) - \varepsilon_{22}(0)$	0.208	0.197	0.125	0.116
$\epsilon(\infty) - \epsilon(0)$	0.430	0.441	0.247	0.261

Table 3.2: Comparison of experimental values and fitted values of Larive's ASR-expansion tests under compressive stress application

kept under the same hygral and thermal conditions as the reactive ones. The strain registered on these samples (due to creep, which for sake of clarity is not considered in this model) was subtracted from the strain measured on the reactive samples. The mean asymptotic strain values, $\delta\varepsilon_{11}(\infty)$ and $\delta\varepsilon_{22}(\infty)$ together with the volume strain $\delta\epsilon(\infty)$, obtained by this operation, are summarized in Table 3.1. In the calibration process of the chemoplastic model, these values are associated with the (mean) asymptotic values of $\varepsilon_{11}(\infty) - \varepsilon_{11}(0)$, $\varepsilon_{22}(\infty) - \varepsilon_{22}(0)$ and $\epsilon(\infty) - \epsilon(0)$ defined by (3.62), (3.63) and (3.64). With α and $\mathbf{b}$ known (see above), the mean value of $\bar{\kappa} = \kappa K_s/K_s'$ can now be determined for the different stress levels (see Table 3.1). In addition, Figure 3.10 shows the mean value of $\bar{\kappa}$ as a function of $\bar{p}_s$. Without the anomalous result of the 10 MPa case, the trend line indicates that $\bar{\kappa}$ decreases with increasing

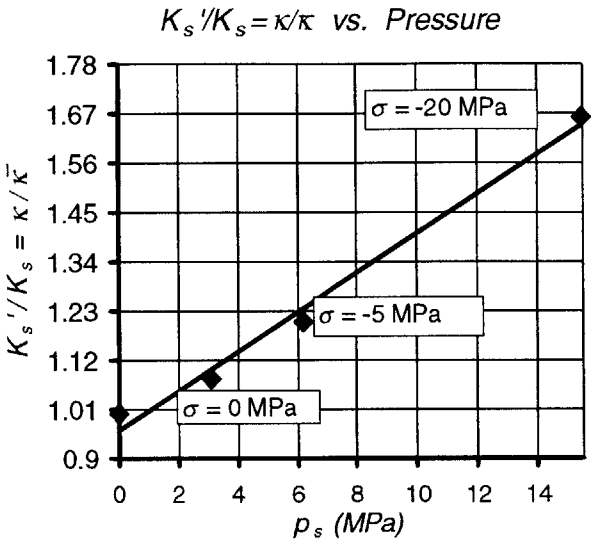

Figure 3.11: Variation of K_s'/K_s with increasing confinement pressure

confinement pressure $\bar{p}_s$. According to (3.60), an extrapolation of this trend line to $\bar{p}_s = 0$ gives a first estimate of $\kappa = \bar{\kappa}$:

$$\kappa = 0.145\% \pm 0.007\% \tag{3.65}$$

Use of (3.65) in (3.60) allows the determination of $K_s'/K_s = \kappa/\bar{\kappa}$ as shown in Figure 3.11. Now (3.60) can be recast as $(\partial K_s/\partial \phi_{s0}^p)\bar{p}_s/K_s^2 = 1 - \kappa/\bar{\kappa}$, which can then be integrated as follows:

$$\frac{dK_s}{K_s^2} = \left(\frac{1-\kappa/\bar{\kappa}}{\bar{p}_s}\right) d\phi_{s0}^p \rightarrow K_s(\phi_{s0}^p) = \frac{K_{s0}}{1 + (\kappa/\bar{\kappa} - 1)\phi_{s0}^p K_{s0}/\bar{p}_s} \tag{3.66}$$

where K_{s0} is a reference value for K_s at $\phi_{s0}^p = 0$, for which $\kappa/\bar{\kappa} = 1 \leftrightarrow \bar{p}_s = 0$. Given the inherent scatter of ASR-test results (e.g. Larive, 1998), the results of this calibration process given in Table 3.2 are reasonably consistent and suggest the following comments:

1. Provided that $K_s > 0$, $\kappa/\bar{\kappa} > 0$ indicates that a plastic hardening phenomenon occurs

according to (3.34):

$$H = \alpha^2 K_s \frac{\kappa}{\bar{\kappa}} \tag{3.67}$$

In the considered loading range with $-\sigma/f_c' \leq 50\%$, the plastic hardening modulus may be assumed constant, i.e., $H = \alpha^2 K_{s0}$, and thus according to (3.66) and (3.67):

$$K_s = K_{s0}\frac{\bar{\kappa}}{\kappa} \leftrightarrow \bar{p}_s = K_{s0}\phi_{s0}^p \tag{3.68}$$

The assumption of a constant hardening modulus is equivalent to assuming a linear increase of ϕ_{s0}^p with $\bar{p}_s$. For $\sigma = 0, -5, -20$ MPa, this is consistent with the constant increase of $K_{s0}/K_s = \kappa/\bar{\kappa}$ with increasing swelling pressure $\bar{p}_s$ shown in Figure 3.11. In turn, for $\sigma = -10$ MPa, the low value of $\kappa/\bar{\kappa} \approx 1$, seems to indicate that the samples had a lower initial porosity on the same order as the stress-free swelling samples.

2. If the initial plastic porosity ϕ_{s0}^p is associated with the volume occupied by the gel before swelling occurs, which in Larive's stress free tests was found by SEM to be on the order of $\phi_{s0}^p \approx 1\%$, K_{s0} can be estimated as 300 MPa. This order of magnitude confirms *a posteriori* the assumption of a negligible chemoelastic deformation, i.e. $\beta/\kappa = K_s/K \ll 1$, where K denotes the overall bulk-modulus.

In summary, Eqn. (3.45), (3.61) to (3.64) and (3.67) allow the determination of the chemo-plastic model parameters. These are the plastic parameters, α and c, and the chemomechanical constants κ and K_s. The plastic parameters can be determined on non-reactive concrete samples, while the chemomechanical parameters require some expansion tests under different stress levels. The values obtained with this calibration process give quite a reasonable fit of Larive's asymptotic strain values. A comparison of experimental and model values is given in Table 3.2.

3.3 Verification of the Calibration Process

The calibration process focused on the asymptotic expansion values. Hence the verification will focus on a comparison of the expansion kinetics, i.e. on the time dependent strain development due to the expansive reaction. The underlying assumption concerning the reaction kinetics is (3.26): the chemical affinity is not affected by stress application. It is written in the dimensionless form:

$$\bar{t}_c \frac{\partial \xi}{\partial \bar{t}} = 1 - \xi \tag{3.69}$$

where $\bar{t} = t/\tau_L$ is the dimensionless time normalized by the latency time τ_L, and $\bar{t}_c$ is the normalized characteristic time function of ASR-swelling defined by (3.13):

$$\bar{t}_c = \frac{t_c}{\tau_L} = \left(\frac{\tau_c}{\tau_L}\right) \frac{1 + \exp[-\tau_L/\tau_c]}{\xi + \exp[-\tau_L/\tau_c]} \tag{3.70}$$

Integrating (3.69) and (3.70) gives:

$$\xi(\bar{t}) = \frac{1 - \exp(-\bar{t})^{\tau_L/\tau_c}}{1 + \exp(1 - \bar{t})^{\tau_L/\tau_c}} \tag{3.71}$$

This result indicates that the development of the reaction extent in time $\bar{t} = t/\tau_L$ depends only on the ratio of time constants τ_L/τ_c.

Provided that $\xi_0 \ll 1$, this implies according to (3.62)–(3.64) that the ASR-expansion also depends only on the time constant ratio τ_L/τ_c. The time constants, τ_L and τ_c, can be determined graphically (Fig. 3.2) from expansion curves defined by the data for a given case of uniaxial stress application at a given reference temperature (here $\theta_0 = 38°C$). Table 3.3 summarizes these results as determined from Larive's expansion tests.

The individual values of the time constants show some scattering, but the time constant

Stress [MPa]	0	-5	-10	-20
$\tau_L(\theta_0 = 38°\text{C})$ [days]	83	66	70	98
$\tau_c(\theta_0 = 38°\text{C})$ [days]	28	22	18	34
τ_L/τ_c [1]	3.0	3.2	3.9	2.9

Table 3.3: Time constants of Larive's ASR-expansion tests under compressive stress application.

ratio τ_L/τ_c appears to be of the same order of magnitude in all experiments, which were carried out under same thermal and hygral conditions. This suggests that the ratio τ_L/τ_c is not strongly affected by macroscopic stress application, and confirms the relevance of the made assumption of the independence of the expansion kinetics on stress application. This is consistent with Larive's microscopic analysis, which showed evidence that the ASR product formation is not affected by stress application. The comparison of experimental values and model values for the longitudinal expansion $\varepsilon_{11}(\bar{t})$ and transverse expansion $\varepsilon_{22}(\bar{t})$ determined from (3.63), (3.64) and (3.71) is given in Figures 3.12a–3.12e. The model values were determined with a time constant ratios shown in Table 3.3, along with the asymptotic values from Table 3.2. Clearly, the predicted expansion matches quite closely with the measured data, thus providing excellent verification of the model calibration process.

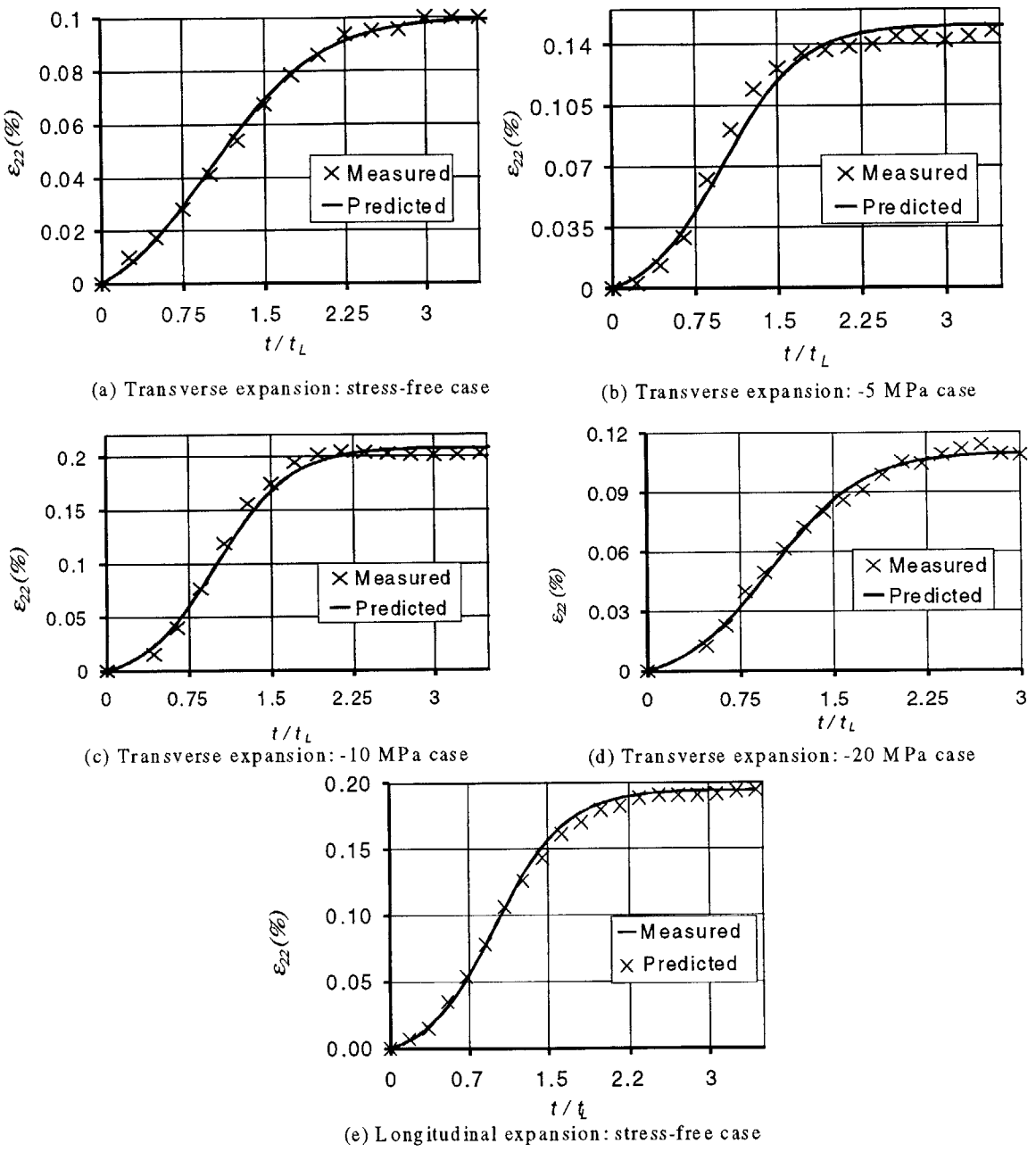

(a) Transverse expansion: stress-free case

(b) Transverse expansion: -5 MPa case

(c) Transverse expansion: -10 MPa case

(d) Transverse expansion: -20 MPa case

(e) Longitudinal expansion: stress-free case

Figure 3.12: Comparison of predicted and measured longitudinal expansion for the various load cases

Chapter 4

Conclusions and Perspectives

Since its identification sixty years ago, the alkali-silica reaction has posed considerable problems for those involved in the construction and maintenance of structures. To date, a comprehensive model that explicitly addresses and accounts for all the chemical and physical mechanisms associated with deleterious reaction has not been presented in the literature. The purpose of this research has been to present a rational, mechanistic model that accurately reproduces the experimentally observable characteristics of ASR with respect to the parameters that affect those characteristics.

Most important among the contributions of this chemoplastic model are the inclusion of irreversible, plastic deformation and consequently the phenomenon of stress-induced anisotropy. Anisotropic expansion resulting from externally applied stress is readily apparent in the ASR expansion data of Larive, but until now has not been modeled in the literature. The chemo-

plastic model employs standard plasticity theory with a Drucker-Prager plasticity criterion to account for this anisotropic behavior. As mentioned at the outset of Chapter 3, the development of this model has consisted of: (1) identification, (2) calibration, and (3) verification. The next logical step in the continuation of this research is the process of model validation, by which the validity of assumptions employed by the model can be checked.

Future research on ASR chemoplasticity might include a more sophisticated, higher-order kinetics law that quantifies such parameters as the reactivity of silica in aggregates and the water content of the concrete. Both of these variables have not been considered explicitly in this model. Further study might involve a closer examination of these parameters and their relative importance to macroscopic expansion. Additionally, a more complex failure surface could be introduced to more precisely predict plastic deformation while continuing to incorporate the effect of stress-induced anisotropy. Furthermore, more data might be collected for *in situ* civil engineering structures, which could then be used to recalibrate the model from application to large scale simulations.

Bibliography

[1] Hobbs, D. W. (1988). *Alkali-silica reaction in concrete.* Thomas Telford Ltd., London.

[2] Stanton, T. E. (1940). Expansion of Concrete Through Reaction between Cement and Aggregate. *Proceedings of the American Society of Civil Engineers.* 66, 1781-1811.

[3] Diamond, S. (1975). A Review of Alkali-Silica Reaction and Expansion Mechanisms: Alkalis in Concrete Pore Solutions. *Cement and Concrete Research.* 5, 329-346.

[4] Taylor, H. F. W. (1997). *Cement Chemistry.* Thomas Telford Ltd., London.

[5] Poole, A. B. (1992). Introduction to alkali-aggregate reaction in concrete. In Swamy, R.N. (Editor).*The Alkali-silica reaction in concrete.* Blackie, London. Chapter 1.

[6] West, G. (1996). *Alkali-aggregate reaction in concrete roads and bridges.* Redwood Books, Trowbridge, Wiltshire.

[7] Ferraris, C. F., Garboczi, E. J., Davis, F. L. and Clifton, J. R. (1997). Effect of Stress Relaxation, Self-Desiccation, and Water Absorption on Alkali-Silica Reaction in Low Water/Cement Ratio Mortars. National Institute of Standards and Technology, Building Materials Division, Gaithersburg, Maryland.

[8] Ferraris, C. F. (1995). Alkali-Silica Reaction and High Performance Concrete. Report NISTIR 5742. National Institute of Standards and Technology, Building and Fire Research Laboratory, Gaithersburg, Maryland.

[9] Glasser, F. P. (1992). Chemistry of the alkali-aggregate reaction. In Swamy, R.N. (Editor).*The Alkali-silica reaction in concrete.* Blackie, London. Chapter 2.

[10] St. John, D. A., Poole, A. W. and Sims, I. (1998). *Concrete Petrography: A handbook of investigative techniques.* Arnold, London.

[11] Swamy, R.N. (1992). Chemistry of the alkali-aggregate reaction. In Swamy, R.N. (Editor).*The Alkali-silica reaction in concrete.* Blackie, London. Chapter 2.

[12] Li, K. (1999). Introduction to Alkali-Aggregate Reaction. Internal Report, Laboratoire des Ponts at Chaussées, Paris.

[13] Chatterji, S. (1989). Mechanisms of alkali-silica reaction and expansion. *Proceedings of the 8th International Conference of the Alkali-Aggregate Reaction in Concrete*, Kyoto. Pp 101-105.

[14] Bažant, Z. P. and Steffens, A. (1999). A Simple Model for the Alkali-Silica Reaction in Concrete. Personal communication to F.-J. Ulm, to be published in *Cement and Concrete Research.*

[15] Dron, R. and Brivot, F. (1992). Thermodynamic and Kinetic Approach to the Alkali-Silica Reaction. Part 1: Concepts. *Cement and Concrete Research.* 22, 941-948.

[16] Dron, R. and Brivot, F. (1992). Thermodynamic and Kinetic Approach to the Alkali-Silica Reaction. Part 2: Experiment. *Cement and Concrete Research.* 23, 93-103.

[17] Dron, R., Brivot, F. and Chaussadent, T. (1997). Mechanism of the Alkali-Silica Reaction. *Proceedings of the 10th International Congress on the Chemistry of Cement*, Gothenburg, Sweden.

[18] Dent-Glasser, L.S. and Kataoka, N. (1981). The Chemistry of 'Alkali-Aggregate' Reaction. *Cement and Concrete Research.* 11, 1-9.

[19] Dent-Glasser, L.S. and Kataoka, N. (1981). A Reply to J. Bensted's Discussion of "The Chemistry of Alkali-Aggregate Reaction". *Cement and Concrete Research.* 11, 809-810.

[20] West, G. and Sibbick, R. G. (1989). A mechanisms for alkali-silica reaction in concrete roads. *Proceedings of the 8th International Conference of the Alkali-Aggregate Reaction in Concrete*, Kyoto. Pp 95-100.

[21] Powers, T.C. and Steinour, H.H. (1955). An Interpretation of Some Published Researches on the Alkali-Aggregate Reaction: Part 1-The Chemical Reactions and Mechanisms of Expansion. *Journal of the American Concrete Institute Proc.* 51, 497-516.

[22] Powers, T.C. and Steinour, H.H. (1955). An Interpretation of Some Published Researches on the Alkali-Aggregate Reaction: Part 2-A Hypothesis Concerning Safe and Unsafe Reactions with Reactive Silica in Concrete. *Journal of the American Concrete Institute Proc.* 51, 785-812.

[23] Dent-Glasser, L.S. and Kataoka, N. (1982). On the role of Calcium in the Alkali-Aggregate Reaction. *Cement and Concrete Research.* 12, 321-331.

[24] Ulm, F.-J., Coussy, O., Li, K. and Larive, C. (2000). Thermo-Chemo-Mechanics of ASR-Expansion in Concrete Structures. *Journal of Engineering Mechanics.* 126, 233-242

[25] Dron, R. and Brivot, F. (1996). Solid-Liquid Equilibrium in K-C-S-H/H2O Systems. *Proceedings of the 10th International Conference of the Alkali-Aggregate Reaction in Concrete*, Melbourne. 927-939.

[26] Dent-Glasser, L.S. (1979). Osmotic Pressure and the Swelling of Gels. *Cement and Concrete Research.* 9, 512-517.

[27] Diamond, S. (1989). ASR-Another look at mechanisms. *Proceedings of the 8th International Conference of the Alkali-Aggregate Reaction in Concrete*, Kyoto. 83-94.

[28] Leger, P., Tinawi, R. and Mounzer, N. (1995). Numerical Simulation of Concrete Expansion in Concrete Dams Affected by Alkali-aggregate reaction: State-of-the-Art. *Canadian Journal of Civil Engineering.* 22, 692-713.

[29] Courtier, R.H. (1990). The Assessment of ASR-Affected Structures. *Cement and Concrete Composites.* 12, 191-201.

[30] Larive, C. (1998). Apports combinés de l'expérimentation et de la modélisation à la comprehension de l'alcali-reaction et de ses effets mécaniques. *Monograph LPC.* OA 28 Laboratoire des Ponts at Chaussées, Paris, France.

[31] Furusawa, Y., Ohga, H. and Uomoto, T. An Analytical Study Concerning Prediction of Concrete Expansion Due to Alkali-Silica Reaction. *Durability of Concrete: Third International Conference.* ACI SP 145-40, 757-778.

[32] Xi, Y., Suwito, A., Wen, X., Meyer, C. and Jin, W. (1999). Testing and Modeling Alkali-silica Reaction and the Associated Expansion of Concrete. *Mechanics of Quasi-Brittle*

Materials and Structures: A Volume in Honor of Z.P. Bažant's 60th Birthday. Hermes Science Publications, Paris, 217-232.

[33] Hashin Z. and Shtrikman, S. (1962). A variational approach to the theory of the effective magnetic permeability of multiphase materials. *Journal of Applied Physics.* 33, 3125-3131.

[34] Coussy, O., Ulm, F.-J., and Mainguy, M. (1999). "Environmental Mechanics of Concrete". Summer-school, Udine, Italy, October, 1999.

[35] Coussy, O. (1995). *Mechanics of Porous Continua.* J. Wiley & Sons, Chicester, U.K.

[36] Chatterji, S. and Christensen, P. (1990). Studies of the Alkali-Silica Reaction: Part 7. Modeling of Expansion. *Cement and Concrete Research*, 20, 285-290.

[37] Pietrusczak, S. (1996) On the Mechanical Behavior of Concrete Subjected to Alkali-Aggregate Reactions. *Computers and Structures.* 58, 1093-1099.

[38] Pietrusczak, S., Jiang, J., and Mirza, F.A. (1988) An Elastoplastic Constitutive for Concrete. *International Journal of Solids and Structures.* 24, 705-722.

[39] Huang and Pietrusczak (1999)Modeling of Thermomechanical Effects of Alkali-Silica Reaction. *Journal of Engineering Mechanics.* 476-485.

[40] Coussy, O. and Ulm, F.-J. (1996). Creep and Plasticity due to Chemo-mechanical Couplings. *Archive of Applied Mechanics*, 66, 523-535.